nature communications

Article

https://doi.org/10.1038/s41467-025-68010-x

High-fat diet disrupts a septal control on feeding to promote obesity in male mice

Received: 24 May 2025

Accepted: 15 December 2025

Published online: 27 December 2025

Check for updates

Shaolei Jiang[1,2,3,9], Shishi Lai[1,4,5,9], Haiyang Jing[1,6], Xiaocong Wu[1,6], Fengling Li[1,6], Bo Chen[1,6], Jin Bao[1], Liping Wang[7], Gaowei Chen[1,6] ✉ & Yingjie Zhu[1,6,8] ✉

The global epidemic of diet-induced obesity poses a significant health challenge. Among brain regions regulating energy homeostasis, the lateral septum has emerged as a critical brake on feeding behavior to prevent overeating. However, the neural adaptations within the septal area under high-fat diet (HFD) and consequent contributions to obesity remain unknown. Utilizing high-throughput single-nucleus RNA sequencing, slice electrophysiology and in vivo calcium imaging, we identified HFD-induced alterations in the transcriptional profiles and neural activity within the septal area of male mice. The HFD suppresses septal neuronal activity by downregulating hyperpolarization-activated cyclic nucleotide-gated channel 1 (Hcn1), and weakens inhibitory control over downstream targets through reduced expression of glutamate decarboxylase 2 (Gad2). Overexpression of Hcn1 and Gad2 enhances septal neuronal activity, restores GABA levels, and prevents HFD-driven overeating and obesity. These findings illustrate how diet disrupts the brain's feeding suppression system, leading to overeating and obesity.

The global obesity prevalence is rapidly increasing, causing serious adverse effects on human health[1,2]. One major factor fueling this epidemic is the widespread accessibility of highly palatable, calorie-dense foods[3–5]. These foods can evoke cravings and engender pleasure, processes regulated by the brain's homeostatic and hedonic feeding systems[6,7]. Hypothalamic neural circuits play a pivotal role in regulating homeostatic feeding driven by hunger, while the brain's reward circuits control hedonic feeding driven by the palatability of food[7–9]. Previous studies identified diet-induced changes in the neuronal excitability, neural inflammation, and transcriptional state of hypothalamic neurons[10–12]. However, how these neural adaptations contribute to the progression of diet-induced obesity remains unknown.

The lateral septum (LS), a brain region rich in GABAergic neurons, has emerged as a critical regulator of feeding behavior[13–18]. As an inhibitory neurotransmitter, GABA and its receptors can modulate food intake, energy homeostasis, and adiposity through complex circuit-specific mechanisms that either promote or suppress feeding depending on the context and target neurons[19–21]. The LS receives substantial inputs from the hippocampus and cortex, and projects to the hypothalamus to generate appropriate behavioral responses, including whether to eat or not[22–24]. Chemogenetic activation of GABAergic neurons in the LS, hippocampal inputs to the LS, and septal projections to the lateral hypothalamic area (LH), all suppress feeding[13,14]. Activation of neurotensin-positive neurons in the LS

[1]Shenzhen Neher Neural Plasticity Laboratory, Shenzhen-Hong Kong Institute of Brain Science, Shenzhen Institutes of Advanced Technology, Chinese Academy of Sciences, Shenzhen, China. [2]Henan Academy of Innovations in Medical Science, Institute of Electrophysiology, Zhengzhou, China. [3]School of Optical-Electrical and Computer Engineering, University of Shanghai for Science and Technology, Shanghai, China. [4]Yunnan University School of Medicine, Yunnan University, Kunming, China. [5]Southwest United Graduate School, Kunming, China. [6]Shenzhen Key Laboratory of Drug Addiction, the Brain Cognition and Brain Disease Institute, Shenzhen Institutes of Advanced Technology, Chinese Academy of Sciences, Shenzhen, China. [7]Shenzhen Key Laboratory of Neuropsychiatric Modulation, the Brain Cognition and Brain Disease Institute, Shenzhen Institutes of Advanced Technology, Chinese Academy of Sciences, Shenzhen, China. [8]Key Laboratory of Biomedical Imaging Science and System, Chinese Academy of Sciences; State Key Laboratory of Biomedical Imaging Science and System, Shenzhen, China. [9]These authors contributed equally: Shaolei Jiang, Shishi Lai. ✉e-mail: gw.chen@siat.ac.cn; yj.zhu1@siat.ac.cn

suppressed overall feeding, whereas inactivation of these neurons specifically promoted hedonic feeding[17,25,26]. Neurotensin-positive neurons in the LS also mediate stress-induced anorexia by responding to stress and suppressing food intake[16]. Activation of glucagon-like peptide 1 receptor (GLP-1R) neurons in the LS suppress feeding and mediate the anorectic effects of liraglutide[18]. Therefore, the LS acts as a regulatory brake within the feeding network, helping to control overeating. Although the critical role of LS in regulating feeding behaviors has been recognized, whether diet can induce molecular and physiological adaptations within the LS and whether these adaptations contribute to diet-induced obesity remains unexplored.

Obesity has a strong genetic underpinning, as evidenced by genome-wide association studies (GWAS) identifying over 1000 loci associated with body mass index (BMI)[27]. Most genes associated with these loci are expressed in the brain, such as leptin receptor (LEPR), melanocortin 4 receptor (MC4R) and SIM BHLH transcription factor 1 (SIM1), indicating obesity as a neurological and mental condition[28]. Pathway-based analyses reveal that the genes are enriched in pathways involved in long-term potentiation, synaptic function, and neurotransmitter signaling (e.g., glutamate and GABA)[29].

By combining single-nucleus transcriptomics, electrophysiology, and in vivo imaging, this study aims to decode high-fat diet (HFD)-induced adaptations in the LS and to elucidate its mechanistic contributions to obesity pathogenesis. We found that, a four-week HFD induced significant transcriptional alterations in septal cells, with GABAergic neurons in the LS (LS^{GABA}) showing most robust gene expression changes and containing the highest concentration of human obesity-associated genes. The HFD decreased the activity of LS^{GABA} neurons and promoted food intake through downregulation of Hcn1 channels. Overexpression of Hcn1 channels restored neuronal excitability, reduced HFD intake and prevented HFD-induced obesity. The HFD also altered inhibitory transmission from LS^{GABA} neurons to lateral hypothalamus and tuberal nucleus via downregulation of Gad2. Overexpression of Gad2 in LS^{GABA} neurons enhanced GABA level and prevented HFD-induced obesity. These results not only illustrate how diet can disrupt the brain's feeding suppression system in the LS and its contribution to the progression of obesity, but also provide molecular and cellular targets for intervening diet-induced obesity.

Results

HFD alters transcriptional profiles of the septal cells

To investigate how HFD-induced obesity modulates the transcriptional profiles of cells within the septal region, adult mice were assigned to either a HFD or control chow diet. Both groups had *ad libitum* access to food. Mice on the HFD exhibited significantly higher energy intake compared to those on the control diet, resulting in a significant increase in bodyweight that surpassed that of control mice as early as the first week (Fig. 1a, b). The caloric intake continued to increase, leading to the development of an obesity phenotype (Fig. 1a, b). After a 4-week dietary regimen, septal tissues were harvested for single-nucleus RNA sequencing (snRNA-seq) (Fig. 1c).

Following quality control (Supplementary Fig. 1a–c), we identified a total of 15,543 cell nuclei from the control group and 19,432 from the HFD group. Subsequently, we categorized 9 cell clusters based on transcriptional profiles and previously reported cell-type markers[30,31]: GABAergic neurons (*Gad1, Gad2*, and *Slc32a1*), astrocytes (*Gja1*), oligodendrocytes (*Mog*), microglia (*Selplg*), oligodendrocyte precursor cells (*Pdgfra*), ependymal cells (*Fam216b*), glutamatergic neurons (*Slc17a6*), endothelial cells (*Flt1*), and mural cells (*Rgs5*) (Fig. 1d and Supplementary Fig. 1d–f). The distribution of cell types was consistent across the control and HFD groups. (Supplementary Fig. 1g).

We then compared differentially expressed genes (DEGs) within each cluster between the HFD and control groups. Notably, GABAergic neurons showed the most significant changes in gene proportion and number (Fig. 1e). We evaluated cell-type signature scores in relation to human obesity-associated gene sets using signatures from DisGeNET[32] and MSigDB[33] databases. Our analysis revealed that there was an enrichment of obesity-related genes in GABAergic neurons (Fig. 1f), with the DEGs of exhibited the most pronounced similarity coefficient with the obesity gene-set (Supplementary Fig. 1h). In GABAergic neurons, the HFD resulted in 2438 downregulated DEGs and 355 upregulated DEGs (Fig. 1g). We next performed cluster analysis for neuronal population and identified seven GABAergic and one glutamatergic cluster (Supplementary Fig. 2a). GABAergic neuronal populations exhibited more downregulated DEGs while the glutamatergic cluster showed more upregulated DEGs (Supplementary Fig. 2b-e). Bioinformatic validation using the Allen Brain Atlas in situ hybridization dataset revealed significant enrichment of marker genes of neuronal populations (e.g., *Cap1, Matn2, Calb2*) within the septal region (Supplementary Fig. 2f). In contrast, striatum-enriched genes (including *Ppp1r1b, Calcr, Upb1*) demonstrated minimal detection in our sequencing profiles (Supplementary Fig. 2g), thereby corroborating the anatomical precision of our dataset. Collectively, these findings demonstrate that HFD drives broad transcriptional adaptations across GABAergic neuronal populations in the septal area.

Gene Ontology (GO) analysis revealed HFD-induced downregulation of synapse functions in GABAergic neurons, particularly impacting synapse structure, synaptic transmission, neurotransmitter secretion, and synaptic plasticity (Fig. 1h and Supplementary Fig. 3a). Gene-concept network analysis focused on neural signaling-related pathways identified 46 interconnected genes, including *Hcn1* and *Npas4*, which are critical for neuronal excitability[34,35], and *Grik2* and *Gabrg2*, essential for synaptic transmission[36,37] (Fig. 1i). Upregulated genes were linked to long-term synaptic depression and lipid metabolism (Supplementary Fig. 3b). These alterations suggest a decline in synaptic transmission and neuronal activity among GABAergic neurons in the septal area by consuming HFD for 4 weeks. Kyoto Encyclopedia of Genes and Genomes (KEGG) analysis showed downregulated genes were associated with glucose metabolism pathways (Fig. 1j), while upregulated genes were involved in lipid metabolism pathways (Supplementary Fig. 3c), suggesting a suppression of glucose metabolism with activation of lipid metabolic pathways.

HFD reduced septal neuronal activity during feeding

Given the dominant distribution of GABAergic neurons in the LS[38–40] and the significant alterations of gene expression in the GABAergic neurons following HFD, we sought to elucidate the impact of HFD on the neural activity of GABAergic neurons in the LS (LS^{GABA}) at cellular resolution in vivo. We injected a Cre-dependent AAV expressing a genetically encoded Ca^{2+} indicator (GCaMP6s) and implanted a gradient index (GRIN) lens into the LS of Gad2-Cre mice (Fig. 2a). Calcium dynamics were subsequently imaged using a head-mounted miniature microscope in free-moving mice 4-6 weeks post-injection. We first characterized the encoding profiles of LS^{GABA} neurons to chow and HFD through randomized food presentation during one imaging session (Fig. 2b). Analysis revealed three distinct response profiles of LS^{GABA} neurons during food consumption: excitatory, inhibitory or non-responsive (403 neurons from 4 mice). Notably, many responsive neurons exhibited food-type selectivity, with 14.1% selective for chow (7.2% excitatory, 6.9% inhibitory), 20.1% for HFD (11.9% excitatory, 8.2% inhibitory), and 13.2% responding to both (8.7% excitatory, 4.5% inhibitory) (Fig. 2c). Next, we performed a population decoding analysis using a linear support vector machine (SVM) classifier to determine whether chow versus HFD trials could be predicted from trial-by-trial neuronal activities during consumption epochs. Activities from all simultaneously imaged LS^{GABA} neurons were z-scored, and principal component analysis (PCA) was applied to reduce dimensionality, retaining the first two principal components (PCs) to represent population activity per trial. A linear SVM was trained on a randomly

https://doi.org/10.1038/s41467-025-68010-x

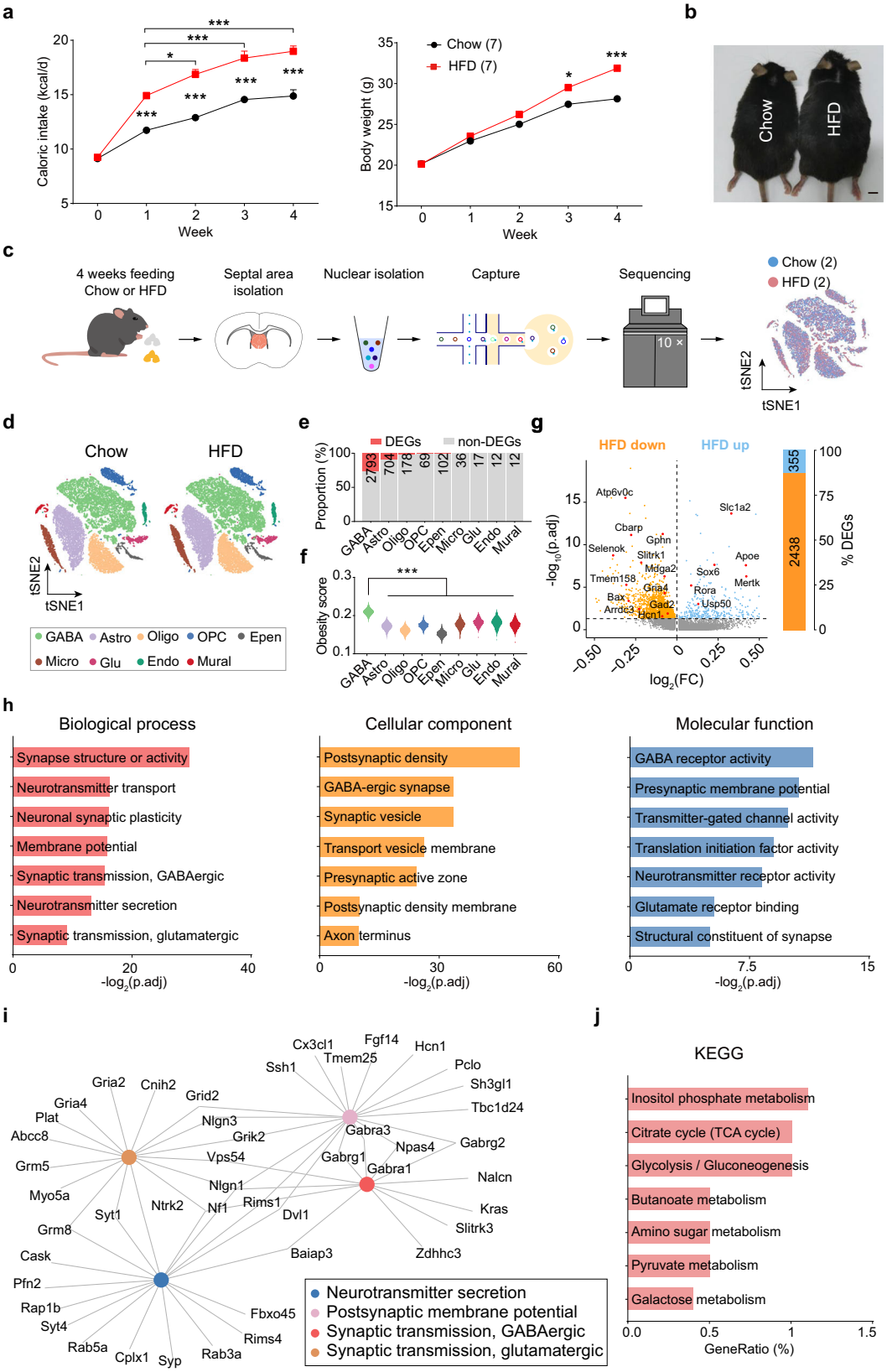

selected 75% of trials from each food type and tested on the remaining 25%, with the process repeated 1000 times to compute average decoding accuracy. Shuffled controls were generated by randomly reassigning trial types. The classifier achieved significantly higher accuracy for actual data compared to shuffled controls, demonstrating that LS^{GABA} population activity encodes sufficient information to distinguish food identities based on palatability or caloric content (Fig. 2d).

We next assessed how diet modulates LS^{GABA} neuronal activity during the consumption of regular food pellet in chow-fed and HFD-fed mice. Two experimental groups underwent 4-week dietary regimens with imaging at day 1 and 30 (Fig. 2e). When the neural activity

Fig. 1 | The HFD alters the transcriptional profiles of septal area neurons. a Left: quantification of daily energy intake for the normal food and high-fat diet groups (diet: $F_{1,60} = 157.2$; $p < 0.001$; time: $F_{4,60} = 132.6$, $p < 0.001$; interaction: $F_{4,60} = 9.5$, $p < 0.001$). Right: quantification of bodyweight between the Chow and HFD groups (diet: $F_{1,60} = 49.3$; $p < 0.001$; time: $F_{4,60} = 196$, $p < 0.001$; interaction: $F_{4,60} = 3.9$, $p < 0.01$). **b** Representative images of the body size of mice after 4 weeks of feeding on chow vs. HFD. Scale bar, 5 mm. **c** Schematic of the snRNA-seq experimental pipeline. **d** tSNE visualization of 9 transcriptionally-distinct clusters from the septal area in the Chow and HFD groups. **e** Percentages of differentially expressed genes (DEGs) and non-differentially expressed genes (non-DEGs) in each cell cluster; the number of DEGs is indicated in the bar. **f** AUC scores for the activity of different cell types from the gene set associated with human obesity ($F_{8,34966} = 24191$, $p < 0.001$). **g** Left: volcano plot of DEGs in LS^{GABA} neurons. Right: proportion of HFD-induced upregulated and downregulated DEGs in LS^{GABA} neurons; the number of DEGs is indicated in the bar. *P* values were adjusted using the Benjamini-Hochberg method for multiple comparisons. **h** HFD-induced downregulated GO pathways in LS^{GABA} neurons. *P* values were adjusted using the Benjamini-Hochberg method for multiple comparisons. **i** HFD-induced downregulated neural signaling gene-concept networks in LS^{GABA} neurons. **j** HFD-induced downregulated KEGG pathways in LS^{GABA} neurons. Statistics: (**a**) two-way ANOVA followed by Sidak's post hoc test, (**f**) one-way ANOVA followed by Tukey's post hoc test, (**g**, **h**) two-sided Mann-Whitney U-test, with detailed statistics provided in Supplementary Data 1. Sample sizes are indicated in the figures. $^{*}p < 0.05$, $^{***}p < 0.001$. Data are presented as mean ± SEM. All tests are two-sided. Source data are provided as a Source Data file.

was aligned with the first bite, about one quarter of the neurons displayed an excitatory response, whereas another quarter exhibited an inhibitory response (Fig. 2f and Supplementary Fig. 4a). The percentage of neurons showing either excitatory or inhibitory response remained unchanged between day 1 and day 30 for both groups (Fig. 2g). The amplitude of both excitatory and inhibitory responses remained unchanged between day 1 and day 30 for chow group (Fig. 2h, i). However, after 4 weeks of HFD, the average amplitude of the excitatory response was reduced, while that of the inhibitory response remained unchanged (Fig. 2j, k). This selective dampening of excitatory responses in HFD-fed mice suggests impaired activation of LS^{GABA} neurons that typically suppress feeding behavior.

HFD alters synaptic transmission and reduces septal neuronal excitability

To investigate the effects of HFD on the synaptic transmission and electrophysiological properties of LS^{GABA} neurons, we selectively labeled these neurons with EGFP by injecting AAV-DIO-EGFP into the LS of Gad2-Cre mice. Electrophysiological recordings in acute brain slices revealed significant alterations in synaptic transmission (Fig. 3a). Specifically, both the amplitude and frequency of spontaneous excitatory post-synaptic currents (sEPSCs) in LS^{GABA} neurons were significantly reduced in the HFD group compared to the chow group (Fig. 3b, c). Furthermore, the paired-pulse ratio (PPR) of electrical stimulation-evoked EPSCs was elevated in the HFD-fed mice, indicating decreased release probability of excitatory inputs (Fig. 3d, e). There was also a small yet significantly lower frequency of spontaneous inhibitory post-synaptic currents (sIPSCs) in the HFD group, although there was no difference in amplitude (Fig. 3f, g). The reduction in the amplitude and frequency of both sEPSCs and sIPSCs was consistent across the LSd, LSi, and LSv subregions (Supplementary Fig. 4b-g). These results indicate that prolonged HFD feeding reduces excitatory inputs onto LS^{GABA} neurons.

We next examined the spontaneous activity and intrinsic excitability of GABAergic neurons in the LS and found that mice in the HFD group had significantly lower spontaneous action potential firing frequency in LS^{GABA} neurons than mice in the chow group (Fig. 3h, i and Supplementary Fig. 4h–k). Step current injections revealed a significant reduction in intrinsic excitability, as shown by a downward shift in the input-output curve (Fig. 3j), with the resting membrane potential and membrane resistance have no change (Fig. 3k, l). Collectively, 4 weeks of HFD decreased excitatory synaptic inputs and reduced intrinsic excitability in LS^{GABA} neurons.

HFD induces downregulation of Hcn1 channels in LS^{GABA} neurons

The reduction of neuronal excitability and spontaneous activity induced by HFD indicates a change in the underlying ion channels that govern firing patterns[41]. To explore potential mechanism, we performed whole-cell patch clamp recordings in LS^{GABA} neurons. Stepwise hyperpolarizing current injections (−200 – 0 pA) elicited a characteristic depolarizing voltage 'sag' (Fig. 4a), a hallmark of hyperpolarization-activated cyclic nucleotide-gated (HCN) cation channel activity. HCN channels mediate inward currents upon activation that critically modulate neuronal excitability[41–43]. Comparisons of the voltage sags revealed a markedly smaller amplitude and lower fraction of neurons exhibiting a substantial voltage sag (> 10% of peak voltage) in the HFD group (Fig. 4a–c), suggesting a decrease in HCN currents following HFD. Perfusion with the selective HCN blocker, ZD-7288 (20 μM), completely blocked the voltage sag, confirming the presence of HCN channels (Fig. 4d).

We then examined our snRNA-seq data, and found that, among four Hcn channel subunits, *Hcn1* exhibited the most pronounced enrichment in septal neurons (Fig. 4e, f). Furthermore, the expression level of *Hcn1* in the LS^{GABA} neurons was significantly downregulated after HFD, although the percentage of neurons with *Hcn1* expression remained unchanged (Fig. 4g, h). To further confirm these findings at the protein level, we performed Hcn1 immunostaining. Compared to mice maintained on a standard chow diet, 4 weeks of HFD indeed led to significantly fewer Hcn1-immunopositive signals in LS^{GABA} neurons, while medial septum neurons showed no significant alteration (Fig. 4i, j and Supplementary Fig. 5).

Downregulation of Hcn1 contributes to hypoexcitability of septal neurons and exacerbates HFD-induced obesity

To evaluate the impact of Hcn1 downregulation on the neuronal excitability of LS^{GABA} neurons and the contribution to HFD-induced obesity, we used short hairpin RNA (shRNA)[44] to knockdown *Hcn1* in LS^{GABA} neurons (Fig. 5a). Immunostaining confirmed effective reduction of Hcn1 protein expression following shRNA expression (Fig. 5b). Whole-cell recordings demonstrated that the *Hcn1* knockdown group had a markedly smaller voltage sag amplitude and a lower proportion of neurons with substantial voltage sag than the control group (> 10% of peak voltage), indicating a decrease in HCN currents (Fig. 5c–e). We next applied depolarizing step currents to evoke action potential firing, and found significantly lower firing frequency in response to 40–120 pA current injections in the *Hcn1* knockdown group, reflecting decreased neuronal excitability (Fig. 5f).

To investigate the role of Hcn1 in feeding behavior, we bilaterally injected AAV-DIO-shRNA (shScr or shHcn1) into the LS of Gad2-Cre mice. Following a three-week period for viral expression, we assessed feeding behaviors using a motorized lick spout with capacitive lick detection, delivering a fixed 10 μL volume of foods with varying palatability (standard liquid food, sucrose solution, or palatable Ensure) (Fig. 5g). In *ad libitum*-fed mice, Hcn1 knockdown did not affect consumption of standard liquid food but significantly increased lick frequency and total intake of palatable sucrose solution and Ensure (Fig. 5h–j)

To explore the role of Hcn1 in HFD-induced obesity, we subjected a distinct cohort of Gad2-Cre mice with Hcn1 knockdown in LS^{GABA} neurons to a four-week HFD or chow diet, starting three weeks after viral injection (Fig. 5k). The caloric intake of mice with Hcn1 knockdown in LS^{GABA} neurons was significantly higher than control mice, and bodyweight gain on the HFD was greater than control mice, whereas Hcn1 knockdown had no effect on the chow-fed mice (Fig. 5l, and Supplementary Fig. 6a). Furthermore, qPCR analysis revealed that,

https://doi.org/10.1038/s41467-025-68010-x

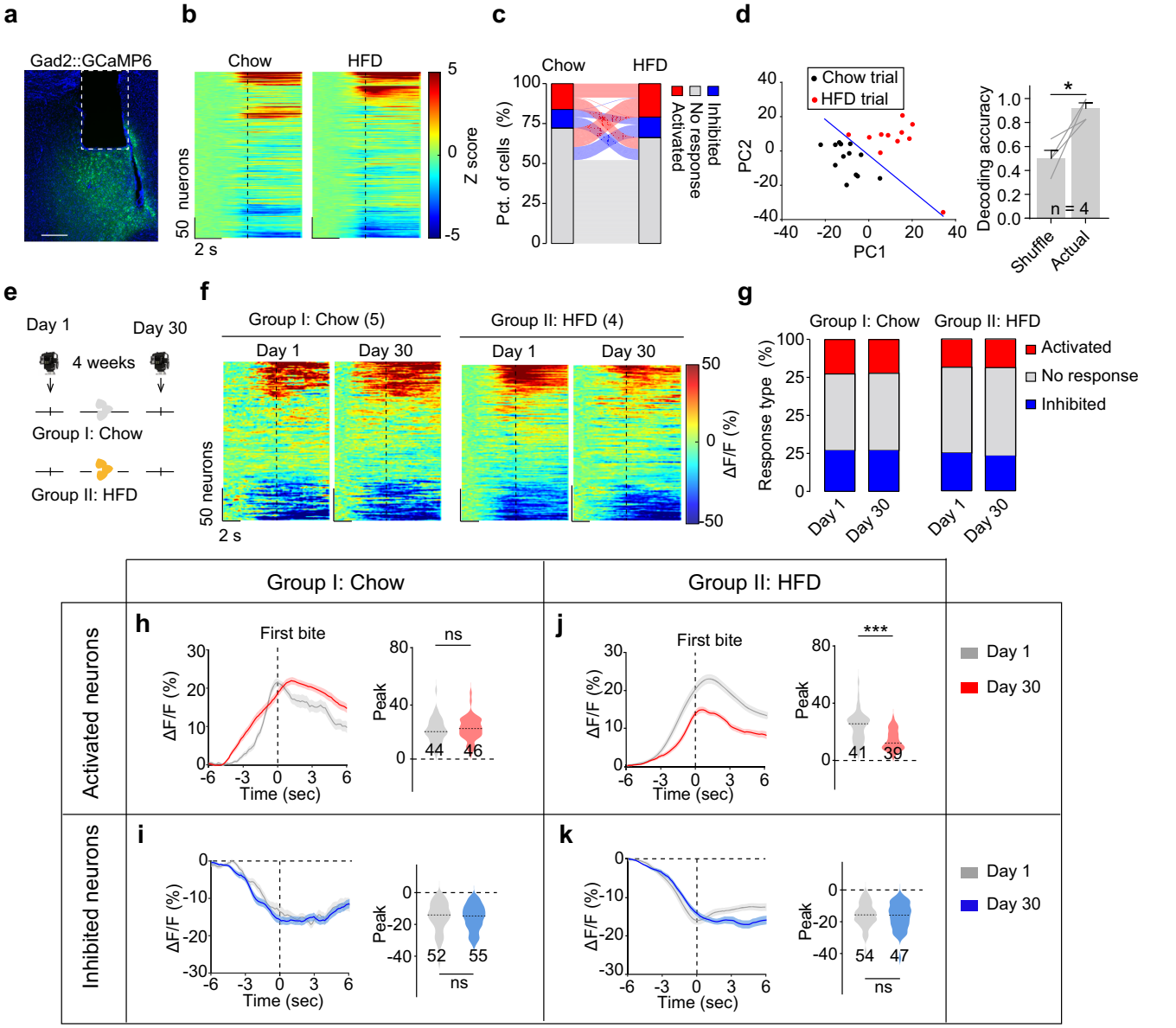

Fig. 2 | The HFD reduces the activity of LS^{GABA} neurons during feeding. **a** Representative image of the viral expression and position of the GRIN lens in the LS. Scale bar, 500 μm. This representative result was confirmed in 9 independent mice. **b** Heatmaps of the LS^{GABA} neurons responses to Chow or HFD. Each row represents the mean activities of one neuron. **c** Sankey diagram showing the response ratio of LS^{GABA} neurons to chow and HFD. **d** Left: example support vector machine (SVM) decoding using neuronal population activities in response to Chow and HFD. Right: performance of decoding using actual neuronal responses to chow and HFD or using neuronal responses shuffled across trial types ($p < 0.05$). **e** Schedule of the miniscope imaging before (Day 1) and after (Day 30) 4 weeks chow (Group I: Chow) or HFD (Group II: HFD) feeding. **f** Heatmaps showing calcium signals at Day 1 and Day 30. The black vertical dashed lines indicate the initiation of feeding behavior. **g** Average traces (left) and quantification of peak (right) of the activated neurons at Day 1 in Group I: Chow and Group II: HFD. **h, i** Average traces (left) and quantification of peak (right) of the activated (**h**) and inhibited (**i**) neurons at Day 1 and Day 30 in Group I: Chow (activated neurons: $p = 0.45$; inhibited neurons: $p = 0.78$). **j, k** Average traces (left) and quantification of peak (right) of the activated (**j**) and inhibited (**k**) neurons at Day 1 and Day 30 in Group II: HFD (activated neurons: $p < 0.001$; inhibited neurons: $p = 0.75$). Statistics: (**d**) two-tailed paired t-test, (**h-k**) two-sided Mann-Whitney U-test, with detailed statistics provided in Supplementary Data 1. Sample sizes are indicated in the figures. ns, no significant difference, * $p < 0.05$, *** $p < 0.001$. Data are presented as mean ± SEM. All tests are two-sided. Source data are provided as a Source Data file.

after four weeks of HFD feeding, the HFD+shHcn1 group exhibited significantly reduced Hcn1 expression compared to the HFD+shScr group (Fig.5m). These findings suggest that Hcn1 knockdown in LS^{GABA} neurons promotes HFD consumption and exacerbates HFD-induced obesity.

Overexpression of Hcn1 restores LS neuronal excitability and prevents HFD-induced obesity

Next, we examine the effect of Hcn1 overexpression on the neuronal excitability of LS^{GABA} neurons and HFD-induced obesity by utilizing adeno-associated virus vectors (Fig. 6a). Immunofluorescence confirmed successful Hcn1 overexpression following this viral strategy (Fig. 6b). Overexpression of Hcn1 led to a significantly higher voltage sag amplitude and enhanced excitability of LS^{GABA} neurons (Fig. 6c–f). In the liquid food intake assays, overexpression of Hcn1 did not affect the standard liquid food intake, but significantly decreased the lick numbers and total intake of palatable sucrose solution and Ensure (Fig. 6g–j). A separate cohort of naïve Gad2-Cre mice were used to test whether Hcn1 overexpression in LS^{GABA} neurons could prevent HFD-induced overeating and obesity.

https://doi.org/10.1038/s41467-025-68010-x

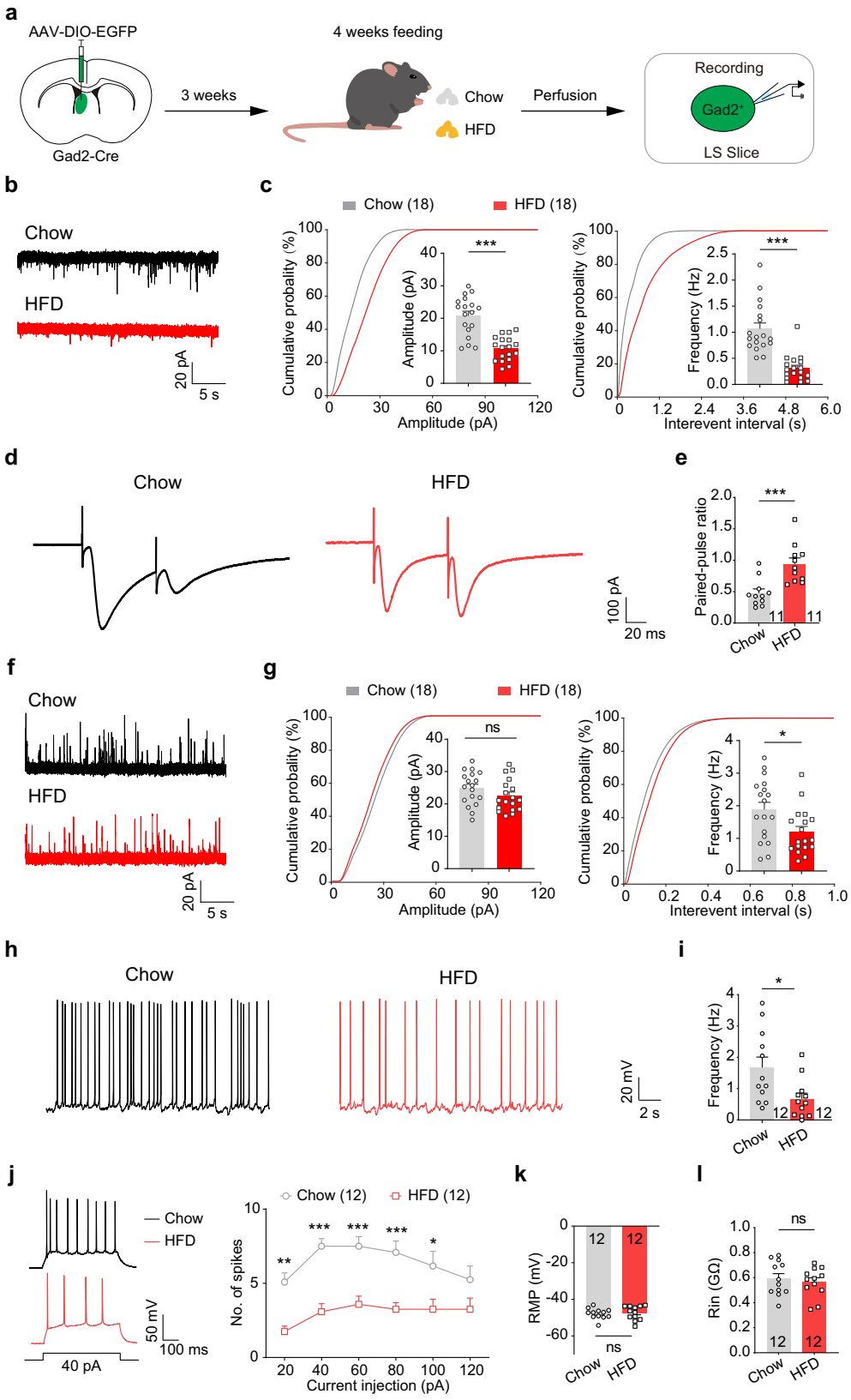

We found mice with Hcn1 overexpression resisted excessive energy intake on an HFD, maintaining bodyweights similar to chow-fed groups and significantly lower than HFD-fed EGFP groups (Fig. 6k, l). Crucially, this metabolic protection was diet-dependent. Overexpression of Hcn1 did not alter food intake or body weight in mice maintained on a standard chow diet (Fig, 6k, l and Supplementary Fig. 6b). qPCR analysis confirmed that Hcn1 expression was significantly higher in the overexpression group after 4 weeks of HFD feeding compared to the Chow+GFP control group (Fig. 6m). These results demonstrate that enhancing Hcn1 channel activity specifically in LS^{GABA} neurons is sufficient to counteract HFD-driven overeating and obesity development.

Fig. 3 | The HFD decreases synaptic transmission in the LS and attenuates the excitability of LS^{GABA} neurons. a Schematic of the patch clamp experimental pipeline. **b** Representative traces of sEPSCs in LS^{GABA} neurons from the Chow and HFD groups. **c** Quantifications of amplitude (left) and frequency (right) of sEPSCs in LS^{GABA} neurons from the Chow and HFD groups (amplitude: $p < 0.001$; frequency: $p < 0.001$). **d, e** Representative traces (**d**) and quantification (**e**) of paired-pulse ratio of electrical stimulation-evoked EPSCs recorded from the Chow and HFD groups ($p < 0.001$). **f** Representative traces of sIPSCs in LS^{GABA} neurons from the Chow and HFD groups. **g** Quantifications of amplitude (left) and frequency (right) of sIPSCs in LS^{GABA} neurons from the Chow and HFD groups (amplitude: $p = 0.15$; frequency: $p < 0.05$). **h** Representative traces of the spontaneous action potential in LS^{GABA} neurons from the Chow and HFD groups. **i** Quantification of action potential firing frequency for the Chow and HFD groups ($p < 0.05$). **j** Left: representative traces at 40 pA current injection in LS^{GABA} neurons from the Chow and HFD groups. Right: quantification of the input-output curves in LS^{GABA} neurons for the Chow and HFD groups (diet: $F_{1,22} = 41.1$; $p < 0.001$; current injection: $F_{5,110} = 3.3$, $p < 0.01$; interaction: $F_{5,110} = 0.98$, $p = 0.43$). **k, l** Quantifications of the resting membrane potential (**k**) and input resistance (**l**) of LS^{GABA} neurons from the Chow and HFD groups (membrane potential: $p = 0.77$; input resistance: $p = 0.74$). Statistics: (**c**, **e**, **g**, **i**, **k**, **l**) two-sided Mann-Whitney U-test, **j** two-way ANOVA followed by Sidak's post hoc test, with detailed statistics provided in Supplementary Data 1. Sample sizes are indicated in the figures. ns, no significant difference, $^{*}p < 0.05$, $^{**}p < 0.01$, $^{***}p < 0.001$. Data are presented as mean ± SEM. All tests are two-sided. Source data are provided as a Source Data file.

Downregulation of Gad2 in the LS contributes to HFD-induced obesity

Beyond the observed reductions in neuronal excitability, our snRNA-seq data also revealed downregulation of synaptic transmission and neurotransmitter secretion in LS^{GABA} neurons following HFD exposure, suggesting potential alterations in the GABA synthesis or releasing. To investigate this hypothesis, we checked our snRNA-seq results and found significantly downregulation of glutamate decarboxylase 2 (*Gad2*) following 4-weeks of the HFD compared to the standard chow diet (Fig. 7a, b). This observation was further validated by quantitative reverse transcription PCR (qPCR) (Fig. 7c). The *Gad2* gene encodes a rate-limiting enzyme that catalyzes GABA synthesis[45]. Reduced *Gad2* expression suggests a compromised GABA synthesis capacity. Consistent with this, liquid chromatograph mass spectrometry (LC-MS) analysis showed significantly lower GABA levels in the LS of HFD mice compared to controls (Fig. 7d).

This reduction of GABA levels in the LS may weaken inhibitory control over downstream brain regions. Using SynaptoTag AAV[46], we mapped the projections of LS^{GABA} neurons (Supplementary Fig. 7a–c) and identified significant synaptic connections to several brain regions, including the preoptic area (POA), the tuberal nucleus (TN), the lateral hypothalamic area (LH), the supramammillary nucleus (SUM), and the ventral tegmental area (VTA) (Supplementary Fig. 7d). Notably, the hypothalamus is widely recognized as a key feeding center. The LH is known to play a crucial role in regulating food intake[7,47], whilst the inhibitory GABAergic pathway from the LS to the LH has been shown to suppress feeding behavior[12,14]. The TN is implicated in hedonic feeding, and our previous studies have reported that activation of the LS→TN pathway specifically enhances the consumption of palatable foods without affecting standard chow intake[17].

To assess the impact of the HFD on GABA transmission from the LS to the LH and TN, we expressed channelrhodopsin-2 (ChR2) in the LS^{GABA} neurons and conducted patch-clamp recordings on LH or TN neurons after 4 weeks HFD or chow feeding (Fig. 7e, f, and Supplementary Fig. 7h–j). Optogenetic stimulation of LS^{GABA} axonal terminals in the LH or TN elicited robust IPSCs, which were blocked by picrotoxin, confirming GABAergic transmission (Fig. 7g). Mice in the HFD group had significantly lower light-evoked IPSC amplitudes (Fig. 7h, i), suggesting reduced GABAergic transmission between the LS and the LH or TN. Furthermore, the PPR of light-evoked IPSC was elevated in HFD-fed mice, indicating decreased presynaptic GABA release probability (Fig. 7j–l). We also found that LS^{GABA} axonal terminals form apparent contacts with distinct neuronal populations in the LH and TN. These putative postsynaptic targets include orexin (ORX)-, melanin-concentrating hormone (MCH)-, and neurotensin (NTS)-postive neurons in the LH and somatostatin (Sst)-postive neurons in the TN (Supplementary Fig. 8). Together, these results demonstrate that GABAergic transmission from LS^{GABA} neurons to the LH and TN, which typically function as a brake to suppress feeding behavior, was weakened following exposure to HFD.

To determine whether reduced GABA release from the LS promotes feeding and weight gain, we employed tetanus neurotoxin (TeNT) to block neurotransmitter release from LS^{GABA} neurons (Fig. 7m). Expression of TeNT effectively blocked GABAergic transmission from the LS to the LH (Supplementary Fig. 9a–d), leading to significantly higher food intake and weight gain on the HFD, but not on the standard chow diet (Fig. 7n and Supplementary Fig. 9e). This indicates that blocking GABA release from LS^{GABA} neurons is sufficient to enhance hyperphagia and accelerate obesity progression under HFD conditions.

To explore whether restoring GABA levels in the LS could rescue HFD-induced obesity, AAV-DIO-Gad2-EGFP was bilaterally injected into LS of Gad2-Cre mice for LS^{GABA} neurons Gad2 overexpression (Fig. 8a). Western blot and LC-MS analyses showed a significant increase in Gad2 and GABA protein in LS (Fig. 8b, c). In the liquid food intake assays, similar to overexpression of Hcn1, overexpression of Gad2 in LS^{GABA} neurons did not affect the standard liquid food intake, but significantly decreased the lick numbers and total intake of sucrose solution and Ensure (Fig. 8d–g). In a distinct cohort of mice, 3 weeks after virus injection, the mice were switched to a 4-week HFD or chow diet. The results demonstrated that Gad2 overexpression in LS significantly reduced HFD intake and prevented obesity (Fig. 8h, i and Supplementary Fig. 10a). Overexpression of Gad2 did not affect chow intake or weight gain (Fig. 8i). qPCR analysis confirmed that Gad2 expression was significantly higher in the overexpression group after 4 weeks of HFD feeding compared to the Chow+GFP control group (Fig. 8j). Importantly, neither silencing of LS^{GABA} neurons, Gad2 overexpression, nor 4-week high-fat diet affected locomotor activity or anxiety-like behaviors (Supplementary Fig. 10b–g). These results indicate that upregulating Gad2 expression in LS^{GABA} neurons is sufficient to prevent overeating and obesity in a HFD context.

Discussion

Overeating and obesity are significant challenges in contemporary health discourse[48]. While previous studies have highlighted the critical role of the LS in regulating feeding behavior, particularly in relation to hedonic feeding and the inhibition of eating[13–15,17,18,23,49], there remains a considerable gap in our understanding of how dietary factors induce neural adaptations within LS cells and how these adaptations contribute to obesity progression. By integrating high-throughput snRNA-seq, electrophysiological recording, and in vivo calcium imaging, our study sheds light on the intricate role of the LS in diet-induced obesity. Specifically, we underscore how HFD triggers transcriptional and functional changes in LS^{GABA} neurons, potentially exacerbating hyperphagia and weight gain (Fig. 1). Our research reveals critical molecular mechanisms underlying the hypoexcitability of LS^{GABA} neurons in response to a HFD, revealing potential therapeutic targets for obesity intervention.

Our findings demonstrate that a HFD leads to significant transcriptional alterations in the septal region, particularly in GABAergic neurons that are enriched with obesity-related genes. Our results suggest that HFD-induced transcriptional alterations within the GABAergic neurons of the septal area may also contribute to human obesity. The downregulation of genes critical for synaptic function and

https://doi.org/10.1038/s41467-025-68010-x

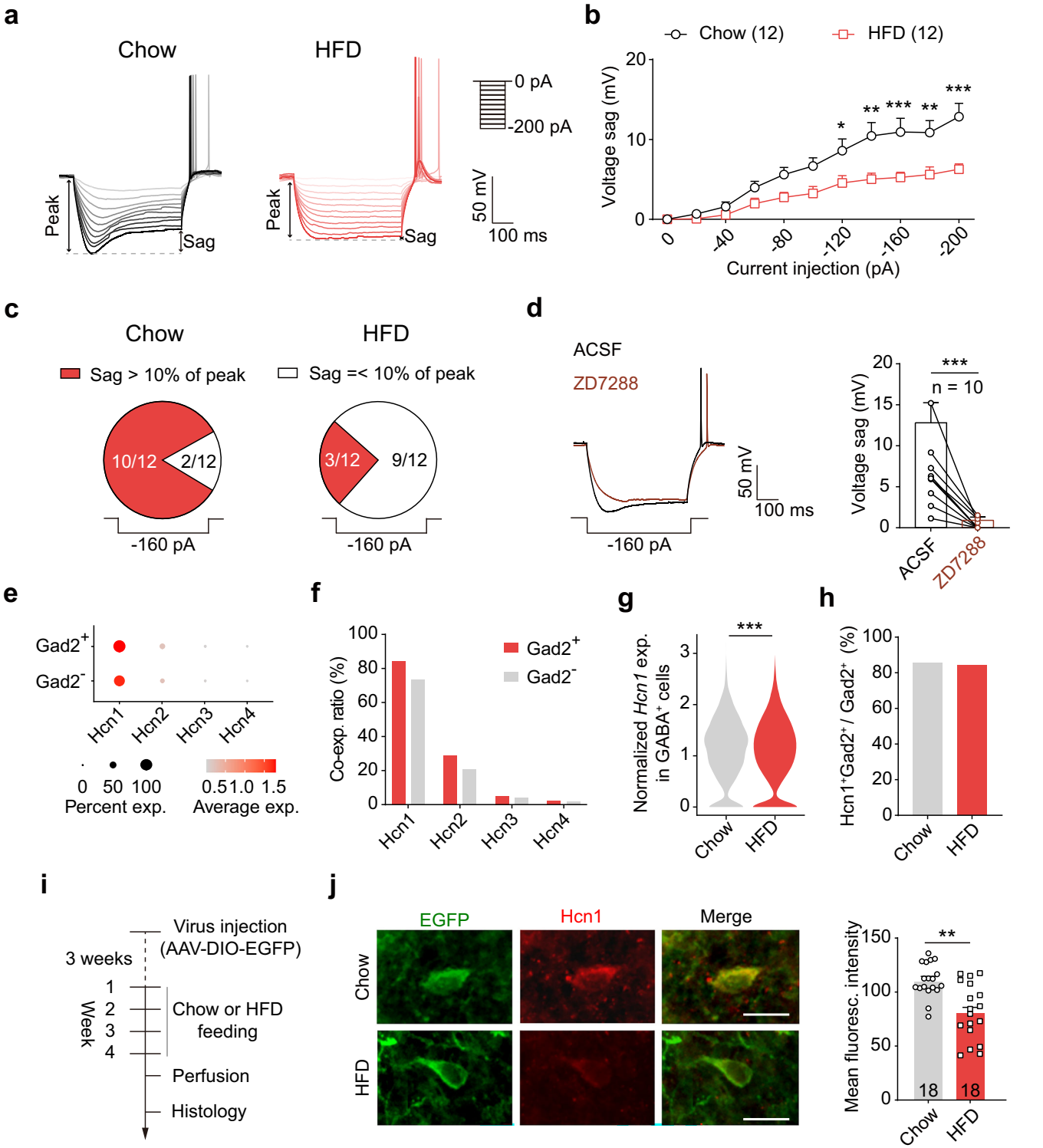

Fig. 4 | The HFD downregulates Hcn1 channels in LS^{GABA} neurons. **a** Representative traces of voltage sag in LS^{GABA} neurons from the Chow and HFD groups. **b** Quantification of voltage sag in LS^{GABA} neurons induced by the step current in LS^{GABA} neurons from the Chow and HFD groups (diet: $F_{1,22} = 12.0$; $p < 0.01$; current injection: $F_{10,220} = 45.7$, $p < 0.001$; interaction: $F_{10,220} = 4.9$, $p < 0.001$). **c** Percentage of LS^{GABA} neurons exhibiting significant voltage sag (>10% of peak voltage) in response to −160 pA current injection in the Chow and HFD groups. **d** Left: representative traces of voltage sag in LS^{GABA} neurons with or without the HCN blocker ZD7288 (20 μM). Right: quantification of voltage sag before and after ZD7288 application ($p < 0.001$). **e** snRNA-seq data showing the Hcn1-4 expression in septal neurons. **f** *Hcn1* expression ratio in Gad2-positive and Gad2-negative neurons in the septal area. **g** Normalized expression of *Hcn1* in LS^{GABA} neurons from the Chow and HFD groups in our snRNA-seq data ($p < 0.001$). **h** Co-expression of *Hcn1* and *Gad2* in septal neurons from the Chow and HFD groups. **i** Timeline for LS^{GABA} neurons Hcn1 protein quantifying following 4 weeks chow or HFD feeding. **j** Left: representative images of Hcn1 expression in LS^{GABA} neurons from the Chow and HFD mice. Scale bars, 10 μm. Right: quantification of Hcn1 protein levels for the Chow and HFD groups ($p < 0.01$). Statistics: (**b**) two-way ANOVA followed by Sidak's post hoc test, (**d**) two-tailed paired t-test, (**g**, **j**) two-sided Mann-Whitney U-test, with detailed statistics provided in Supplementary Data 1. Sample sizes are indicated in the figures. *$p < 0.05$, **$p < 0.01$, ***$p < 0.001$. Data are presented as mean ± SEM. All tests are two-sided. Source data are provided as a Source Data file.

https://doi.org/10.1038/s41467-025-68010-x

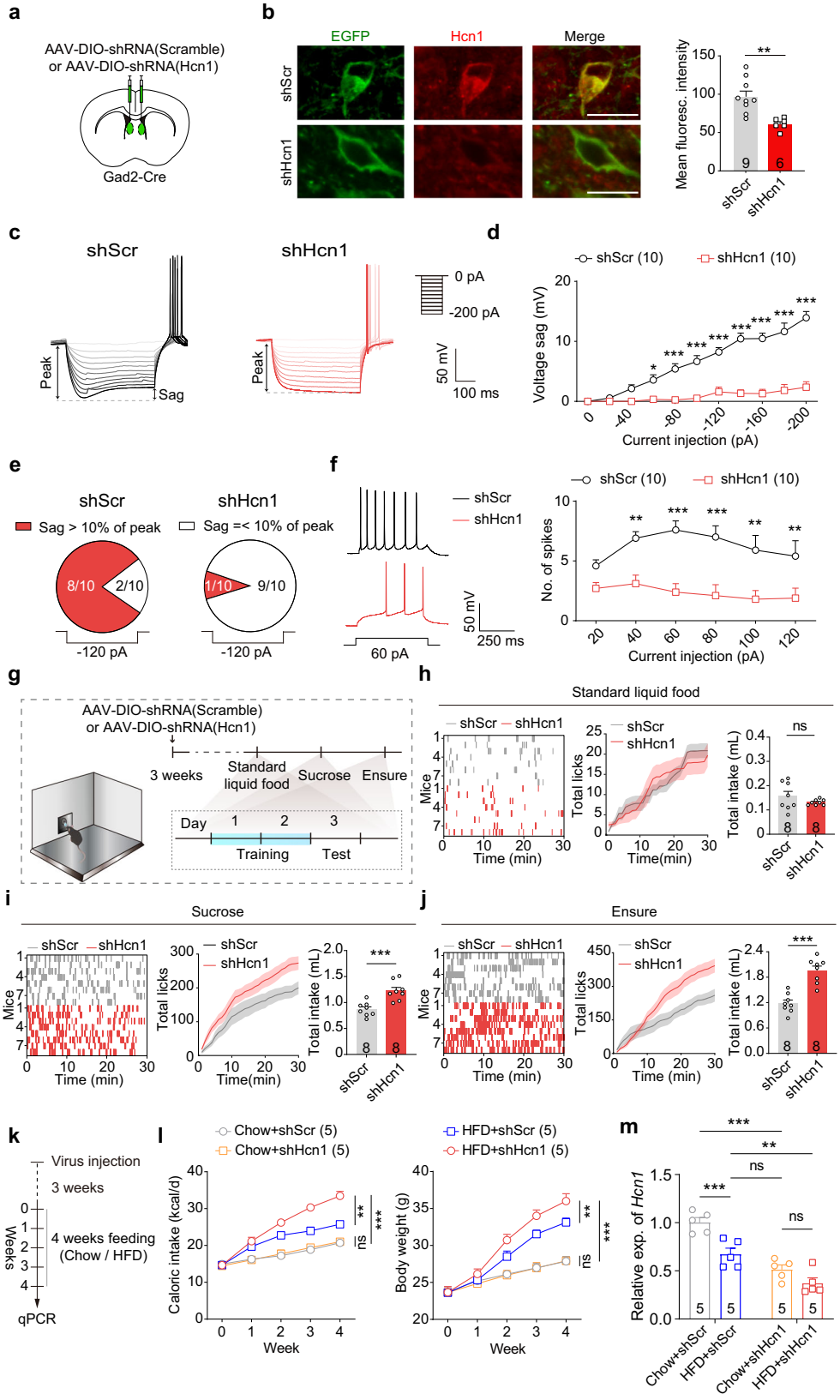

neuronal excitability, such as Gad2 and Hcn1, suggests a disruption in the ability of the LS to regulate feeding behavior (Fig. 1). These transcriptional changes correlate with functional deficits, as evidenced by reduced synaptic transmission and decreased excitability of LS^{GABA} neurons (Figs. 2, 3). Such alterations undermine the ability of the LS to act as a regulatory brake on food intake, particularly under hedonic feeding conditions driven by palatable diets. This emphasizes the notion that, while the brain orchestrates feeding behavior, consumed foods can significantly reshape the brain's feeding network.

A critical highlight of our study is the role of the gene Gad2, a candidate gene for human obesity[50,51], which our results show is significantly affected by the HFD. The diet diminishes GABA synthesis in

Fig. 5 | Knockdown of Hcn1 in the LS promotes HFD-induced obesity. a Viral strategy for *Hcn1* knockdown in LS^{GABA} neurons. **b** Left: representative images of Hcn1 expression in LS^{GABA} neurons from the control (shScr) and Hcn1-knockdown (shHcn1) groups. Right: quantification of Hcn1 protein levels ($p < 0.01$). Scale bars, 10 μm. **c** Representative voltage sag traces in LS^{GABA} neurons in response to hyperpolarizing steps. **d** Quantification of sag amplitude (virus: $F_{1,18} = 65.2$; $p < 0.001$; current injection: $F_{10,180} = 48.8$, $p < 0.001$; interaction: $F_{10,180} = 24.6$, $p < 0.001$). **e** Percentage of LS^{GABA} neurons showing significant sag (> 10% of peak). **f** Left: representative traces at 60 pA current injection. Right: Input–output curves for LS^{GABA} neurons (virus: $F_{1,18} = 20.3$; $p < 0.001$; current injection: $F_{5,90} = 2.1$, $p = 0.07$; interaction: $F_{5,90} = 1.7$, $p = 0.14$). **g** Schematic of the experimental design. **h–j** Liquid food intake in shScr vs. shHcn1 mice. Left: licking behavior; middle: cumulative licks; right: total intake of standard liquid food (**h**), sucrose solution (**i**) and Ensure (**j**) (standard liquid food: $p = 0.78$; sucrose solution: $p < 0.001$; Ensure: $p < 0.001$). **k** Timeline for HFD/chow study with Hcn1 knockdown. **l** Energy intake (left) and body weight (right) across groups [Energy intake (virus: $F_{1,16} = 404.8$, $p < 0.001$; diet: $F_{1,16} = 43.2$; $p < 0.001$; time: $F_{2.768,44.29} = 89.1$, $p < 0.001$). Body weight (virus: $F_{1,16} = 10.4$, $p < 0.01$; diet: $F_{1,16} = 145.2$; $p < 0.001$; time: $F_{1.872,29.95} = 2095$, $p < 0.001$)]. **m** *Hcn1* expression level (virus: $F_{1,16} = 52.8$, $p < 0.001$; diet: $F_{1,16} = 18.9$; $p < 0.001$; interaction: $F_{1,16} = 3.1$, $p = 0.1$). Statistics: (**b**, **h–j**) Mann-Whitney U-test, (**d**, **f**) two-way ANOVA followed by Sidak's post hoc test, (**m**) two-way ANOVA followed by post hoc test using two-stage step-up method of Benjamini, Krieger and Yekutieli, (**l**) three-way ANOVA followed by post hoc test using two-stage step-up method of Benjamini, Krieger and Yekutieli, with detailed statistics provided in Supplementary Data 1. Sample sizes are indicated in the figures. ns, no significant difference, $^{*}p < 0.05$, $^{**}p < 0.01$, $^{***}p < 0.001$. Data are presented as mean ± SEM. All tests are two-sided. Source data are provided as a Source Data file.

the LS by downregulating Gad2, weakening inhibitory control exerted by LS^{GABA} neurons on the LH and TN (Fig. 7)[52,53]. This finding suggests that dietary composition can have profound biological effects on neural circuits critical for feeding regulation.

The downregulation of Hcn1 channels appears pivotal in mediating the reduced excitability and activity of LS^{GABA} neurons. This aligns with previous studies illustrating the role of HCN channels in maintaining neuronal excitability and rhythmic firing[43,54]. Our data indicate that Hcn1 knockdown exacerbates caloric intake and weight gain under HFD conditions, while Hcn1 overexpression restores neuronal excitability and mitigates these effects (Figs. 4–6). This underscores the potential of targeting ion channel pathways to modulate neuronal activity and counteract HFD-induced obesity. The diminished excitability, synergized with decreased GABA synthesis, results in weakening the 'feed-brake' from the LS onto downstream regions, including LH.

Our results corroborate previous findings that highlight the pivotal role of the LS in regulating hedonic feeding[17]. Specifically, synaptic silencing, overexpression of Gad2 or Hcn1, and Hcn1 knockdown exert effects selectively in the context of palatable foods, such as the HFD, sucrose and Ensure, but not the standard chow. Prior literatures have shown that somatostatin neurons in the tuberal nucleus (TN^{Sst}) enable environmental contexts to drive hedonic feeding[17]. Furthermore, LS^{GABA} neurons serve as upstream regulators of TN^{Sst} neurons[17,55]. This connectivity suggests that HFD-induced diminished inhibition from LS^{GABA} neurons may disinhibit TN^{Sst} neuron, thereby promoting hedonic feeding. The lack of effect on chow intake is consistent with the dominant role of hypothalamic circuits (e.g., the arcuate nucleus) in governing homeostatic feeding. Collectively, these insights underscore the LS as a key nodal point in motivational neural circuits, offering targets for interventions in disorders of overconsumption like obesity.

Furthermore, a noteworthy finding of our study is the identification of three distinct subpopulations of LS^{GABA} neurons exhibiting divergent responses to feeding—namely, excitation, inhibition, or no response (Fig. 2)—with many responsive neurons showing food-type selectivity for chow versus HFD (Fig. 2c, d). This functional diversity highlights specialized encoding of food palatability in LS^{GABA} neurons, with implications for distinguishing hedonic (palatable food-driven) from homeostatic feeding. Under HFD conditions, dampened excitatory responses likely contribute to hyperphagia by weakening inhibitory control over downstream circuits such as the LH and TN.

Previous studies have established the hippocampus and hypothalamus as major sources of excitatory inputs to LS^{GABA} neurons, whose activation reduces feeding[13,56]. We employed rabies virus (RV)-mediated, cell-type-specific transsynaptic tracing and confirmed the existence of these specific circuit connections (Supplementary Fig. 7e-g). These findings align with our observation of weakened excitatory inputs to LS^{GABA} neurons after HFD (decreased sEPSC frequency and amplitude, increased PPR), suggesting that such inputs may originate from the hippocampus, hypothalamus or other related structures. Whether HFD leads to decreased excitability of hippocampal or hypothalamic glutamatergic neurons and its impact on LS^{GABA} neurons warrant further investigation.

Studies have demonstrated significant sex differences in the responses of mice and humans to HFD, with females generally exhibiting greater resistance to diet-induced obesity compared to males[57,58]. Given that some LS neurons express estrogen receptors[43,59]—which could modulate neuronal excitability in a sex-dependent manner—future research should therefore investigate potential sex differences in diet-induced neural adaptations in the LS and their contribution to sex-dependent obesity.

In conclusion, our study not only advances the understanding of how a HFD can disrupt brain's feeding suppression system, but also identifies potential molecular targets for therapy. By elucidating the roles of Gad2 and Hcn1 in LS^{GABA} neurons, we pave the way for novel interventions in treating eating disorders and obesity, emphasizing the therapeutic potential of modulating brain circuits to address these widespread health challenges.

Methods

Animals

In this study, adult male C57BL/6 J mice were obtained from the Guangdong Medical Laboratory Animal Center, Guangzhou, China. Additionally, the experimental cohorts included Gad2-Cre (male, Jax No. 010802) mice. All mice were housed in a temperature (22–25 °C) and humidity (55–65%) controlled environment, with ad libitum access to food and water, except during experimental sessions. A 12-hour light-dark cycle was maintained (lights on from 7:00 am to 7:00 pm). All efforts were made to minimize animal suffering and the number of animals used. A total of 338 mice were used in the different experiments. All experiments were conducted in accordance with relevant guidelines and regulations, and approved by the IACUC (Institutional Animal Care and Use Committee) of SIAT, Chinese Academy of Sciences (CAS, SIAT-IACUC-230927).

Diets

The high-fat diet pellet (60% fat, 15% protein, 25% carbohydrate) was purchased from Shenzhen Ready Biological Medicine Co., Ltd (Shenzhen, China, Cat# D12492). The standard chow diet (9% fat, 15% protein, and 76% carbohydrate) was purchased from Beijing Keao Xieli Feed Co., Ltd (Beijing, China, Cat# 2252). Diet was provided ad libitum in each group.

Stereotaxic surgeries

Stereotaxic injections were carried out on mice under anesthesia with isoflurane (3% induction, maintained at 1–1.5%) using a stereotaxic device (RWD Life Science Co., LTD., China). Ophthalmic ointment was placed on the eyes, and topical anesthetic (lidocaine) was applied to

https://doi.org/10.1038/s41467-025-68010-x

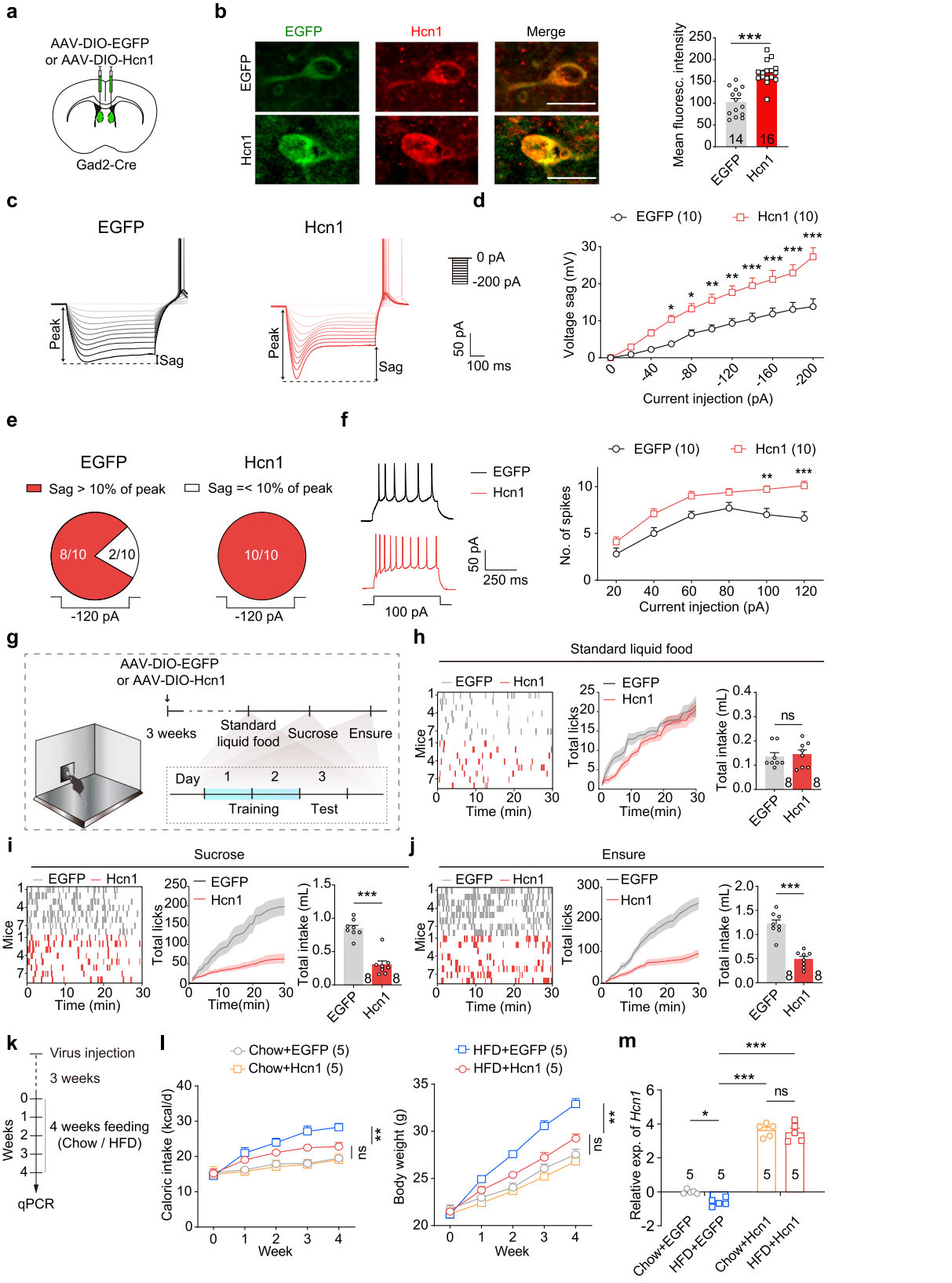

the incision site. A pulled glass capillary attached to a pressure nanoinjector (Drummond Scientific Company) was used to inject 200 nl of AAV virus solution into the LS (AP: +0.5 mm, ML: ±0.45 mm, DV: −2.8 mm) at a slow rate (60 nl/min). The injection needle was left in place for 10 min after the injection was completed.

For calcium imaging, unilateral injections of AAV2/9-hEF1a-DIO-GCaMP6s (Taitool Bioscience, S0351-9) were performed. A GRIN lens was inserted 100 μm above the injection site and secured to the skull with dental cement.

Fig. 6 | Overexpression of Hcn1 in the LS reduces HFD-induced obesity. a Viral strategy for Hcn1 overexpression in LS^{GABA} neurons. **b** Left: representative images of Hcn1 protein levels from the LS^{GABA} neurons in the EGFP (Control) and Hcn1 (Hcn1-overexpression) groups. Scale bars, 10 μm. Right: quantification of Hcn1 protein levels ($p < 0.001$). **c** Representative voltage sag traces in response to hyperpolarizing steps. **d** Quantification of sag amplitude (virus: $F_{1,18} = 14.9$; $p < 0.01$; current injection: $F_{10,180} = 117$, $p < 0.001$; interaction: $F_{10,180} = 8.6$, $p < 0.001$). **e** Percentage of LS^{GABA} neurons showing significant sag (> 10% of peak). **f** Left: representative traces at 100 pA current injection. Right: Input–output curves for LS^{GABA} neurons (virus: $F_{1,18} = 19.2$; $p < 0.001$; current injection: $F_{5,90} = 39.1$, $p < 0.001$; interaction: $F_{5,90} = 1.4$, $p = 0.22$). **g** Schematic of the experimental design. **h-j** Liquid food intake in EGFP vs. Hcn1-overexpressing mice. Left: licking behavior; middle: cumulative licks; right: total intake of standard liquid food (**h**), sucrose solution (**i**) and Ensure (**j**) (standard liquid food: $p = 0.94$; sucrose solution: $p < 0.001$; Ensure: $p < 0.001$). **k** Timeline for HFD/chow study with Hcn1 overexpression. **l** Energy intake (left) and body weight (right) across groups [Energy intake (virus: $F_{1,16} = 3.4$, $p = 0.08$; diet: $F_{1,16} = 48.8$; $p < 0.001$; time: $F_{2.876,46.02} = 142.9$, $p < 0.001$). Body weight (virus: $F_{1,16} = 4.8$, $p < 0.05$; diet: $F_{1,16} = 48.9$; $p < 0.001$; time: $F_{1.835,29.36} = 447.7$, $p < 0.001$)]. **m** *Hcn1* expression level. Data were natural log-transformed to satisfy parametric assumptions (virus: $F_{1,16} = 5.2$, $p < 0.05$; diet: $F_{1,16} = 575$; $p < 0.001$; interaction: $F_{1,16} = 2.2$, $p = 0.16$). Statistics: (**b**, **h**–**j**) Mann-Whitney U-test, (**d**, **f**) two-way ANOVA followed by Sidak's post hoc test, (**l**) three-way ANOVA followed by post hoc test using the two-stage step-up method of Benjamini, Krieger and Yekutieli, (**m**) two-way ANOVA followed by post hoc test using the two-stage step-up method of Benjamini, Krieger and Yekutieli, with detailed statistics provided in Supplementary Data 1. Sample sizes are indicated in the figures. ns, no significant difference, $^{*}p < 0.05$, $^{**}p < 0.01$, $^{***}p < 0.001$. Data are presented as mean ± SEM. All tests are two-sided. Source data are provided as a Source Data file.

For optogenetics activation of LS^{GABA} neurons, unilateral injections of AAV2/9-hEF1a-DIO-hChR2(H134R)-EGFP (Taitool Bioscience, S0858-9) were administered.

For Hcn1 and Gad2 overexpression, AAV2/9-hSyn-DIO-EGFP (Taitool Bioscience, S0746-9), AAV2/9-hEF1a-DIO-Hcn1 (Taitool Bioscience, WY4046), or AAV2/9-hSyn-DIO-EGFP-P2A-GAD2 (BrainVTA, PT-5664) was bilaterally injected into the LS of Gad2-Cre mice. For Hcn1 knockdown, AAV-hSyn-DIO-mClover3-shRNA (Scramble) (Brain Case, BC-2315) or AAV-hSyn-DIO-mClover3-shRNA (mHcn1) (Brain Case, BC-2314) was bilaterally injected into LS.

For pathway tracing, AAV2/9-hSyn-FLEX-tdTomato-T2A-synaptophysin-EGFP (Taitool Bioscience, S0161-9) was infused into the LS. Histological examinations were carried out three weeks post-administration.

For synaptic inactivation, AAV2/9-hEF1a-DIO-mCherry (Taitool Bioscience, S0197-9) or AAV2/9-hEF1a-DIO-mCherry-P2A-TetTox (Taitool Bioscience, S0506-9) was bilateral injected into the LS.

Mice were monitored daily and allowed to recover for at least one week before any food manipulation and at least three weeks prior to any manipulations to allow for viral infection.

Single-nuclei RNA seq and data analysis

The mice were anesthetized with isoflurane, and the brain tissue from the septal area was extracted. All tissue harvested were transferred to −80 °C freezer for storage. Subsequently, the samples were further processed and subjected to single-nuclei RNA sequencing by OE Biotech Co., Ltd. (Shanghai, China) in a process carried out, with some adjustments, to previously established methods[60]. Mouse brain nuclei were processed using a droplet-based 3′ end protocol with the Chromium Next GEM Single Cell 3′ Reagent Kits v3.1 from 10x Genomics. The library was prepared with the Chromium Single Cell 3′/5′ Library Construction Kit, following the manufacturer's precise instructions. Sequencing was performed on the Illumina Nova 6000 system. And we obtained at least 100 GB of raw data per library. Data analysis was conducted using the Cell Ranger software suite version 3.1.0 from 10x Genomics, which demultiplexed the barcodes, aligned reads to the reference genome and transcriptome with the STAR aligner, and normalized the data. This resulted in a detailed matrix correlating gene expression levels to individual cells.

The raw data was processed and analyzed using Seurat (version 5.0)[61]. The data was filtered, with cells having fewer than 200 genes, UMI less than 500, or more than 5% mitochondrial gene transcripts being removed. The 'DoubletFinder' tool facilitated the removal of doublets[62]. Sample integration was accomplished through canonical correlation analysis reduction, with the 2000 most variably expressed genes in each sample, identified via a variance-stabilizing transformation, serving as anchor features[63]. For cell type clustering, the integrated expression matrices underwent scaling and centering, succeeded by principal component analysis (PCA) for dimensionality reduction. The initial fifteen principal components (PC1-PC15) were then utilized to construct nearest-neighbor graphs. To delineate discrete cell populations, Louvain clustering was implemented, with a resolution parameter set at 0.1. The visualization of these clusters was facilitated through t-stochastic neighbor embedding (tSNE). Cluster-specific marker identification was performed using the 'FindAllMarkers' function. To investigate HFD-induced transcriptional alterations, differential expression analysis was conducted using the 'FindMarkers' function. *P* values were adjusted using the Benjamini-Hochberg correction method for multiple testing correction. Functional enrichment analysis, including GO and KEGG pathway assessments, was systematically performed using the 'clusterProfiler' package[64].

To calculate obesity signature score. The obesity gene set was defined based on pathways associated with human obesity and being overweight, as cataloged in DisGeNET[32] (C0028754, C1561826, C4237343, and C0497406) and MSigDB[33] (HP_ABDOMINAL_OBESITY, HP_ABNORMALITY_OF_BODY_MASS_INDEX) datasets. We employed the R package AUCell[65] to calculate the signature score for the obesity-related gene set, which is ranking-based, and independent of the gene expression units and the normalization procedure. Initially, we constructed a ranked expression matrix utilizing the 'AUCell_buildRankings' function, followed by the calculation of the area under the curve (AUC) value through the 'AUCell_calcAUC' function.

Electrophysiological recordings

Procedures for preparing acute brain slices were similar to those described previously[66]. Mice were anesthetized with isoflurane. Under sterile conditions, we perfused the mice with 4 °C slicing solution containing (in mM) 110 choline chloride, 2.5 KCl, 0.5 $CaCl_2$, 7 $MgCl_2$, 1.3 NaH_2PO_4, 1.3 Na-ascorbate, 0.6 Na-pyruvate, 25 glucose, and 25 $NaHCO_3$), then placed the tissue in 4 °C slicing solution saturated with 95% O_2 and 5% CO_2. Coronal slices (250–300 μm) containing the LS, LH or TN were prepared using a vibratome (Leica, VT-1000S). Slices were incubated in 37 °C oxygenated artificial cerebrospinal fluid (in mM: 125 NaCl, 2.5 KCl, 2 $CaCl_2$, 1.3 $MgCl_2$, 1.3NaH_2PO_4, 1.3 Na-ascorbate, 0.6 Na-pyruvate, 25 glucose, and 25 $NaHCO_3$) for at least 30 min for recovery. Then the slices were transferred to a recording chamber and superfused with 2 ml min^{-1} artificial cerebrospinal fluid. Recording was performed at room temperature (23 °C) with a Multiclamp 700B amplifier and a Digidata 1550B acquisition system (Molecular Devices). Data were sampled at 10 kHz and analyzed with Clampfit (Molecular Devices) or MATLAB (MathWorks).

For whole-cell voltage-clamp recordings, patch pipettes (3–5 MΩ) pulled from borosilicate glass (BF 150-86-101.50 mm 0.86 mm 250 px 250, Sutter) were filled with a Cs-based low Cl^- internal solution containing (in mM) 135 $CsMeSO_3$, 10 HEPES, 1 EGTA, 3.3 QX-314, 4 Mg-ATP, 0.3 Na-GTP, 8 Na_2-phosphocreatine, 290 mOsm kg^{-1}, adjusted to pH 7.3 with CsOH. For current-clamp recordings, the internal solution contained (in mM) 130 K-gluconate, 10 KCl, 10 HEPES, 1 EGTA, 2 Mg-ATP, 0.3 Na-GTP, 2 $MgCl_2$, 290 mOsm kg−1, adjusted to pH 7.3 with KOH. Action potential firing was examined by applying a series of long

depolarizing sweeps (500 ms) at 20 pA steps (20 pA–120 pA). Voltage sag was induced by executing a polarization protocol (−200 pA–0 pA, step = 20 pA, duration = 500 ms). To record spontaneous excitatory postsynaptic currents (sEPSCs), picrotoxin was added to ACSF to block GABA receptors. ACSF without any supplements was used for excitatory PPRs recording. PPRs were evoked by electrical stimulation of the LS (0.2-ms current pulses) at a holding potential of −70 mV, and calculated as the ratio of the second electrical stimulation-evoked EPSC to the first electrical stimulation-evoked EPSC, with an interstimulus interval of 50 ms. To record spontaneous inhibitory postsynaptic currents (sIPSCs). CNQX (10 μM) and APV (50 μM) were added to ACSF to block AMPA and NMDA receptors, respectively. To record light-

Fig. 7 | The HFD diminishes LS^{GABA} neuron-mediated inhibition in downstream hypothalamic regions. a Schematic of septal tissue dissection after 4-week chow/HFD feeding. **b**–**d** *Gad2* mRNA and GABA protein levels in LS were decreased after HFD, as shown by snRNA-seq (**b**, $p < 0.001$), qPCR (**c**, $p < 0.01$), and LC-MS (**d**, $p < 0.05$). **e** Representative images of ChR2 expression in LS and axonal terminals in hypothalamus. Scale bars, 500 μm. This pattern of expression and projection was consistently observed across 6 mice. **f** Experimental setup for recording postsynaptic currents in LH or TN upon optogenetic stimulation of LS^{GABA} axons. **g** Representative light-evoked IPSCs in slices from the Chow and HFD groups, which can be blocked by picrotoxin (PTX). **h**, **i** Quantifications of light-evoked IPSCs in LH (**h**) and TN (**i**) [LH (diet: $F_{1,18} = 28.3$, $p < 0.001$; light power: $F_{1.549,27.88} = 79.7$; $p < 0.001$; interaction: $F_{3,54} = 6.7$, $p < 0.001$). TN (diet: $F_{1,22} = 14.4$, $p < 0.001$; light power: $F_{3,66} = 57.6$; $p < 0.001$; interaction: $F_{3,66} = 3.6$, $p < 0.05$)]. **j** Representative paired-pulse ratio (PPR) traces. **k**, **l** Quantifications of the PPR of light-evoked IPSCs in LH (**k**) and TN (**l**) from the Chow and HFD groups (LH: $p < 0.001$; TN: $p < 0.001$). **m** Viral strategy and timeline for silencing LS^{GABA} neurons. **n** Energy intake (left) and body weight (right) in control (EGFP) vs. TeNT groups under Chow/HFD [Energy intake (virus: $F_{1,28} = 11.2$, $p < 0.01$; diet: $F_{1,28} = 91.7$; $p < 0.001$; time: $F_{3.51,98.4} = 71.8$, $p < 0.001$). Body weight (virus: $F_{1,28} = 17.7$, $p < 0.001$; diet: $F_{1,28} = 96.6$; $p < 0.001$; time: $F_{2.07,57.9} = 475$, $p < 0.001$)]. Statistics: (**b**–**d**, **k**, **l**) Mann-Whitney U-test, (**h**, **i**) two-way ANOVA followed by Sidak's post hoc test, (**n**) three-way ANOVA followed by post hoc test using two-stage step-up method of Benjamini, Krieger and Yekutieli, with detailed statistics provided in Supplementary Data 1. Sample sizes are indicated in the figures. ns, no significant difference, $^{*}p < 0.05$, $^{**}p < 0.01$, $^{***}p < 0.001$. Data are presented as mean ± SEM. All tests are two-sided. Source data are provided as a Source Data file.

evoked IPSCs, TTX (1 μM), 4-AP (100 μM), CNQX (10 μM) were added to ACSF. Within the optogenetic stimulation protocol, a blue light pulse (470 nm, 2 ms, 1–4 mW) was delivered through an optical fiber to illuminate the entire field of view. The light-emitting diode (470 nm, Thorlabs) was controlled by digital commands from the Digidata 1550B. Next, the PPR of light-evoked IPSCs was recorded at a holding potential of 0 mV. IPSCs were induced by blue light stimulation (2-ms light pulses) targeting the region containing the recorded cells, and the PPR was calculated as the ratio of the second light-evoked IPSC to the first light-evoked IPSC, with an interstimulus interval of 100 ms. To block IPSCs, picrotoxin (100 μM) was added into recording chamber through a perfusion system and incubated for at least 5 min.

Single-cell calcium imaging

After 4-6 weeks of GCaMP6s injection, a baseplate that matched the miniscope (UCLA Miniscope V4, Open Ephys)[67] was fixed to each mouse's skull with dental cement. Before imaging sessions, mice received 10-minute adaptive training for at least 3 days. During the imaging session, we randomly placed a food pellet for each freely moving mouse in turn, and simultaneously recorded video of the process whereby the mouse ate the food. There were at least 10 food intake periods during the whole imaging session. Imaging data were acquired at a 30-Hz frame rate and collected using UCLA Miniscope-DAQ-DT-Software.

Calcium signal processing was performed using CNMF-E software to extract motion-corrected GCaMP6s fluorescence dynamics from individual neurons[68,69]. Neuronal activity traces were quantified as Z-scores or ΔF/F values, with baselines defined as the mean fluorescence during the first 2 seconds of each trial. To classify neuronal response types, we compared trial-specific fluorescence peaks/troughs against baseline signals. Significant responses were identified using Wilcoxon signed-rank tests ($P < 0.05$): neurons with positive peaks were classified as "activated", those with negative peaks as "inhibited", and non-significant responses ($P \geq 0.05$) as "no response".

For population-level analysis of LS GABAergic neuronal encoding to chow versus HFD, we employed population vector analysis[70]. In brief, this approach constructs n-dimensional activity vectors (n = neuron count) representing ensemble responses at each timepoint through Z score normalized signals. PCA was subsequently applied for dimensionality reduction, projecting high-dimensional vectors onto a 2D visualization space.

Decoding analysis. Population decoding analysis was performed using a linear support vector machine (SVM) classifier in MATLAB (via the 'fitcsvm' function) to assess whether trial types (chow vs. HFD consumption) could be predicted from trial-by-trial population activities of LS^{GABA} neurons during consumption epochs. For each imaging session per mouse, we included the calcium activity traces from all simultaneously imaged neurons. First, neuronal activities were z-scored across trials to normalize the data. Principal component analysis (PCA) was then applied to the matrix of z-scored trial-by-trial activities, and the first two principal components (PCs) were retained to represent low-dimensional population activity patterns for each trial. Next, the dataset was split such that a randomly selected subset comprising 75% of trials from each food type (chow and HFD) served as the training set, while the remaining 25% constituted the test set. Using the low-dimensional PC data from the training set, a linear-kernel SVM classifier ('linear') was trained for two-class decoding (chow vs. HFD trials). The trained classifier was then validated using the 'predict' function to classify the trial-by-trial activities in the test set, yielding a classification accuracy for that iteration. For control purposes, shuffled datasets were generated by randomly reassigning trial-type labels (chow or HFD) to the neuronal activities while preserving the original data structure. The same PCA, training/testing split, and classification procedures were applied to these shuffled data. To ensure robustness, the entire classification process—including random train/test splitting, classifier training, testing, and shuffling—was repeated 1000 times for both the actual and shuffled datasets. The final decoding accuracy was computed as the average classification rate across these 1000 iterations, with significance evaluated by comparing actual accuracies against the shuffled distribution.

qPCR

The septal area tissues were harvested after 4 weeks of either standard chow or HFD and were immediately frozen in liquid nitrogen and stored at −80 °C. The total RNA was extracted using the RNAprep Pure Tissue Kit (TIANGEN, DP431) and reverse-transcribed into cDNA libraries using the PrimeScript™ RT reagent Kit (Perfect Real Time) (Takara, RR037A) according to the manufacturer's instructions. The qPCR was performed using SYBR Premix Ex TaqII (Takara, RR820A). The signals were detected using Quant Studio3 (Applied Biosystems) under the following conditions: 50 °C for 2 min, 95 °C for 10 min, 40 cycles of 95 °C for 15 sec and 60 °C for 1 min, followed by a dissociation stage.

The specific primer sequences used for detection of target genes are listed below:

Gad2:
Forward: 5′-GGCTCTGGCGATGGAATCTT′,
Reverse: 5′-ATGGAATCATTTTCCCTCTCTCG′.
18sRNA:
Forward: 5′-CGCCGCTAGAGGTGAAATTCT-3′,
Reverse: 5′-CGAACCTCCGACTTTCGTTCT-3′.
Hcn1:
Forward: 5′-CACTTCGTATCGTGAGGTTTACA′,
Reverse: 5′-GGGCAGCTGCATATTTACTCTC-3′.

The expression of Gad2 in HFD group relative to the control group was calculated by the ΔΔCT method using 18sRNA as the reference gene. Data were natural log-transformed to satisfy parametric assumptions in Hcn1 and Gad2 overexpression experiments (Figs. 6m, 8j)[71].

https://doi.org/10.1038/s41467-025-68010-x

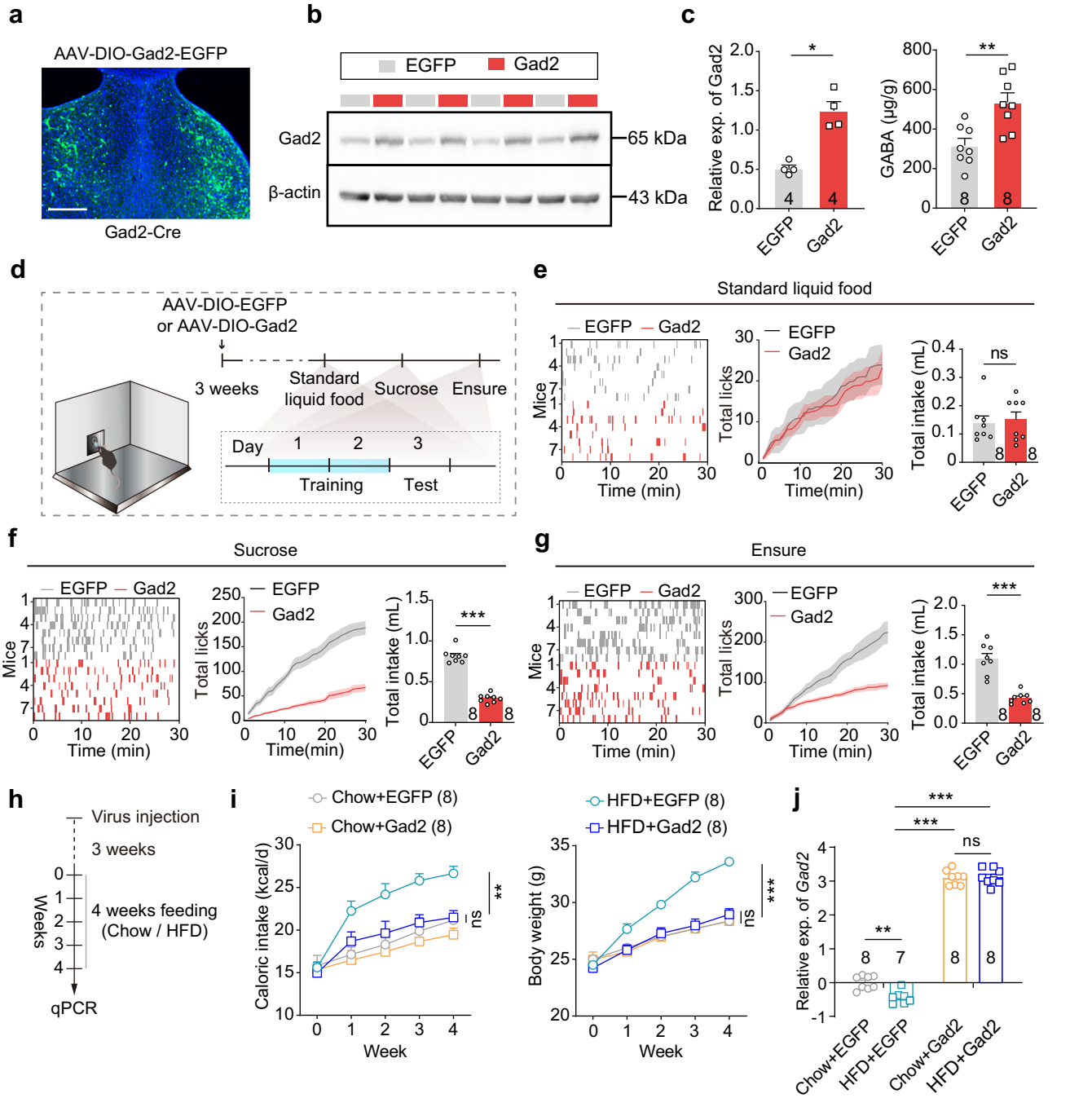

Fig. 8 | Downregulation of Gad2 in LS^{GABA} neurons contributes to HFD-induced obesity. a Representative image of AAV-DIO-Gad2 expression in the LS. Scale bar, 500 μm. This pattern of expression and projection was consistently observed across 3 independent biological replicates. **b** Left: western blot analysis of Gad2 expression in the EGFP (Control) and Gad2 (Gad2 overexpression) groups (β-actin was an internal reference). Right: quantification of Gad2 signal intensity for the EGFP and Gad2 groups ($p < 0.05$). **c** Quantification of GABA expression levels for the EGFP and Gad2 groups ($p < 0.01$). **d** Schematic of the experimental design. **e**–**g** Liquid food intake in EGFP vs. Gad2-overexpressing mice. Left: licking behavior; middle: cumulative licks; right: total intake of standard liquid food (**e**), sucrose solution (**f**) and Ensure (**g**) (standard liquid food: $p = 0.94$; sucrose solution: $p < 0.001$; Ensure: $p < 0.001$). **h** Viral strategy and timeline for overexpression Gad2 in LS^{GABA} neurons. **i** Quantification of energy intake (left) and body weight (right) for the Chow+EGFP, Chow+Gad2, HFD + EGFP, and HFD+Gad2 groups [Energy intake (virus: $F_{1,28} = 18.1$, $p < 0.001$; diet: $F_{1,28} = 29.8$; $p < 0.001$; time: $F_{3.08,86.25} = 33.3$, $p < 0.001$). Body weight (virus: $F_{1,28} = 10.1$, $p < 0.01$; diet: $F_{1,28} = 10.5$; $p < 0.01$; time: $F_{1.848,51.75} = 219.9$, $p < 0.001$)]. **j** Quantification of *Gad2* expression level (virus: $F_{1,27} = 6.2$, $p < 0.05$; diet: $F_{1,27} = 1895$; $p < 0.001$; interaction: $F_{1,27} = 7.9$, $p < 0.01$). Statistics: (**b**, **c**, **e**–**g**) Mann-Whitney U-test, (**i**) three-way ANOVA followed by post hoc test using two-stage step-up method of Benjamini, Krieger and Yekutieli, (**j**) two-way ANOVA followed by post hoc test using two-stage step-up method of Benjamini, Krieger and Yekutieli, with detailed statistics provided in Supplementary Data 1. Sample sizes are indicated in the figures. ns, no significant difference, $^*p < 0.05$, $^{**}p < 0.01$, $^{***}p < 0.001$. Data are presented as mean ± SEM. All tests are two-sided. Source data are provided as a Source Data file.

LC-MS

Mice were anesthetized with isoflurane, and septal area were rapidly dissected at a 4 °C environment. For the LC-MS analytical procedure, samples (8–13 mg) were pulverized in a glass container following the addition of 200 μl of ice-cold methanol containing 0.1% formic acid and 100 μg/ml of vitamin C (VC) in methanol. After vortexing the mixture for 15 min, it was subjected to centrifugation at 12,000 × *g* for 15 min at 4 °C. Post-centrifugation, the clear liquid above the sediment was carefully decanted and then dried using a nitrogen gas flow. From this solution, a 10 μl sample was taken and introduced into a LC-MS system (Shimadzu LCMS-8060, Kyoto, Japan) for analysis. The separation of the analytes was achieved using a BEH C18 column (2.1 mm × 100 mm, 1.7 μm, Waters, Milford, USA). GABA levels were quantified utilizing the external standard method[72].

Western Blot

The mice were anesthetized with isoflurane and the septal area was extracted on ice. The tissue was digested and homogenized in chilled N-PER lysis buffer (Thermo Fisher Scientific, 87792) consisting of phosphatase inhibitor (Roche, 04906837001) and proteinase inhibitor (MCE, K0010). The samples were centrifuged at 12,000 × *g* at 4 °C for 15 min, and the supernatants were collected. We determined the protein concentration of the samples using a BCA protein assay kit (Invitrogen, 23227), and adjusted the protein concentration of each sample to 3 μg/μL. Then we mixed the supernatants with the SDS-PAGE Sample Loading Buffer (biosharp, BL502B), vortex thoroughly, and denatured by boiling. Supernatants (15 μL) were loaded into a 10% SDS-PAGE gel at 80 V for 30 min, followed by 120 V for 100 min. The separated proteins were then transferred onto PVDF membranes (Merck-Millipore, IPVH00010), blocked with 5% skimmed milk for 2 hr at room temperature, and incubated in primary antibody overnight at 4 °C. After washing, membranes were subsequently incubated with secondary antibody for 2 hr at room temperature. We then briefly incubated the membranes with a chemiluminescence reagent (PerkinElmer, NEL104001EA) and detected the signals using ChemiDoc (Bio-Rad). Relative protein expression was estimated by normalizing with the β-actin. The band densities were analyzed using ImageJ software.

The primary antibodies used were rabbit anti-Gad65 (1:3000, Proteintech, Cat# 20746-1-AP) and mouse anit-β-actin (1:3000, Proteintech, Cat# 66009), The secondary antibodies used were goat anti-rabbit (1:2000, ThermoFisher, Cat# 32460) or goat anti-mouse (1:2000, ThermoFisher, Cat# 62-6520).

Histology and immunohistochemistry

Tissue preparation. Mice were deeply anesthetized with pentobarbital sodium and perfused transcardially with 1× PBS at room temperature, followed by 4% paraformaldehyde (PFA) in 1× PBS. Brains were removed and postfixed in 4% PFA overnight at 4 °C, then cryoprotected in 15% and 30% sucrose solutions until they sank. Coronal brain sections (50 μm or 20 μm) were cut on a cryostat (Leica).

Virus-mediated neural tracing. To trace the downstream projections of LS^{GABA} neurons, AAV2/9-hSyn-FLEX-tdTomato-T2A-synaptophysin-EGFP-WPRE-pA was injected into the LS. Brain sections from these mice were obtained following the procedures described above. For immunostaining, brain sections were rinsed with PBS (3 × 10 min) and then blocked with 10% normal goat serum and 0.3% TritonX-100 in PBS for 2 hr at room temperature. Next, sections were incubated with primary antibody (Rabbit anti-GFP, 1:1000, ThermoFisher, Cat# A-11122) diluted in 10% normal goat serum and 0.3% TritonX-100 in PBS for 24–48 hr at 4 °C. After washing with PBS (3 × 10 min), sections were incubated with secondary antibody (Goat anti-Rabbit 488, 1:1000, ThermoFisher, Cat# A-11008) diluted in 10% normal goat serum and 0.3% Triton X-100 in PBS at room temperature for 2 hr and then counterstained with DAPI (1:3000).

Hcn1 immunohistochemistry. For verification of Hcn expression level, immunofluorescent staining for Hcn1 were performed. After the feeding procedure, brain sections (50 μm) from these mice were obtained. Then the brain sections were incubated with primary antibody (Rabbit anti-Hcn1, Proteinech, Cat# 55222-1-AP, 1:100) overnight at 4 °C. Then the brain sections were also washed and incubated with secondary antibodies (Goat anti-Rabbit 555, ThermoFisher, Cat# A32727, 1:1000,) and DAPI, following the previously described procedures[43].

To determine the proportion of ORX, MCH, Nts, Sst, Vglut2, and Vgat expressing neurons among those projecting from the LS to the LH or TN. Rabbit anti-Orexin (1:200, Cell Signaling, #16743) and Rabbit anti-MCH (1:1000, abcam, #ab274415) were used as primary antibodies for the immunofluorescent labeling of orexin and MCH producing neurons. Commercially available and validated RNAscope probes from Advanced Cell Diagnostics were used to target the following mRNAs: Nts (Cat# 420441), Sst (Cat# 404631), Vgat (Cat# 319191-C3), and Vglut2 (Cat# 319171-C2). Tissue sections (20 μm) were processed using the RNAscope Multiplex Fluorescent V2 Assay (Cat# 323100), integrated with an immunofluorescence co-detection workflow, according to the manufacturer's instructions. For GFP immunofluorescence, a rabbit anti-GFP primary antibody (1:200, Thermo Fisher, A-11122) and an Alexa Fluor 488-conjugated goat anti-rabbit secondary antibody (1:500, Thermo Fisher, Cat# A-11008) were diluted in a dedicated co-detection antibody diluent (Cat# 323160) for incubation. The images were acquired with a slide scanner (Olympus Virtual Slide Microscope, VS120-S6-W) and then cell counting was performed with custom-written MATLAB code.

Behavioral tests

Mice were housed in groups (3–5 per cage) for at least 3 weeks following virus injection or fiber implantation before behavioral tests. Mice were handled daily at least 3 days before behavioral tests. The experimenters were blind to the treatment conditions and rated all behaviors. All behavioral experiments were carried out at least three times in the laboratory.

Food intake and bodyweight measurements. Mice were housed individually for at least three days before food intake tests. Feeding behavior trials involved daily replacement of food (standard chow or high-fat pellet, ~20 g) and cage changes to prevent food debris from accumulating at the bottom. Food intake was manually calculated in the home cage during the early dark phase (8:00 p.m. - 10:00 p.m.) by quickly removing the food from the cages and weighing it. To avoid the potential effects of stress caused by diet change, mice were acclimated to the new diet for at least three days before experiments.

For bodyweight measurement, after virus injections, mice were housed in groups (3–5 animals per cage) fed with the standard chow. After 3 weeks, bodyweight was measured once per week. Next, mice were fed either standard chow or high-fat diet. For liquid food intake assays, lick-triggered delivery experiments were conducted using three liquid foods: (1) a standard liquid diet formulated based on the AIN-93M formula (Shenzhen Ready Biological Medicine Co., Ltd.); (2) a 15% (w/v) sucrose solution; and (3) a 25% (w/v) milk powder solution (Ensure). Prior to testing, mice had ad libitum access to solid food and water. During experiments, mice were individually housed in an operant conditioning chamber (22 × 16 × 15 cm; AniLab). Liquids were dispensed via a syringe pump, with licks detected by a custom lickometer incorporating a capacitive touch sensor (SparkFun MPR121) and an Arduino microcontroller. Each detected lick triggered the delivery of a 10-μL droplet. For each food type, mice underwent 2 days of training (30 min/session), followed by a 30-min consumption test on day 3.

Open-field test. Mice were habituated to the experimental room for 3 hours prior to the commencement of behavioral assays. The

apparatus was cleaned between each mouse with a 20% ethanol solution to nullify potential residual olfactory cues. Mice were subsequently introduced to a square open-field arena (each side 40 cm). Mouse trajectories were captured by an overhead camera at 30 Hz for 5 min using a MATLAB-based tracking algorithm. For analytical purposes, the chamber was conceptually bifurcated into two zones: a central quadrant (20 cm × 20 cm) and a peripheral domain. Parameters recorded for analysis included overall locomotor activity and the proportion of time spent within the central area.

Statistics

Data were processed and analyzed using MATLAB, R and GraphPad Prism 9.1.0. Three-way ANOVA followed by post hoc test using the two-stage step-up method of Benjamini, Krieger and Yekutieli to compare more than two experimental groups with time, diet and virus variables. Two-way ANOVA followed by the post hoc Sidak's test was used to compare more than two experimental groups with time variables. One-way ANOVA followed by post hoc Tukey's test was used to compare more than two experimental groups without time variables. Mann-Whitney test or two-tailed unpaired t-test was used to compare two groups without time variables. Data were presented as mean ± SEM. Statistical significance levels are indicated as follows: $^{*}p < 0.05$, $^{**}p < 0.01$, $^{***}p < 0.001$.

Reporting summary

Further information on research design is available in the Nature Portfolio Reporting Summary linked to this article.

Data availability

The raw sequence data generated in this study have been deposited in the Genome Sequence Archive[73] in National Genomics Data Center[74], China National Center for Bioinformation / Beijing Institute of Genomics, Chinese Academy of Sciences (GSA: CRA020474) that are publicly accessible at https://ngdc.cncb.ac.cn/gsa. Source data are provided with this paper.

Code availability

The code used in the snRNA-seq analysis is available online on GitHub (https://github.com/ZhuLab-SZ/Jiang_et_al_2025).

References

1. Flier, J. S. Obesity wars: molecular progress confronts an expanding epidemic. *Cell* **116**, 337–350 (2004).
2. Van Hoeken, D. & Hoek, H. W. Review of the burden of eating disorders: mortality, disability, costs, quality of life, and family burden. *Curr. Opin. Psychiatry* **33**, 521–527 (2020).
3. Hohos, N. M. & Skaznik-Wikiel, M. E. High-fat diet and female fertility. *Endocrinology* **158**, 2407–2419 (2017).
4. *Diagnostic and statistical manual of mental disorders: DSM-5™, 5th ed.* (American Psychiatric Publishing, Inc., 2013).
5. Treasure, J., Duarte, T. A. & Schmidt, U. Eating disorders. *Lancet* **395**, 899–911 (2020).
6. Saper, C. B., Chou, T. C. & Elmquist, J. K. The need to feed: homeostatic and hedonic control of eating. *Neuron* **36**, 199–211 (2002).
7. Stuber, G. D., Schwitzgebel, V. M. & Luscher, C. The neurobiology of overeating. *Neuron* **113**, 1680–1693 (2025).
8. Rossi, M. A. & Stuber, G. D. Overlapping brain circuits for homeostatic and hedonic feeding. *Cell Metab.* **27**, 42–56 (2018).
9. Alcantara, I. C., Tapia, A. P. M., Aponte, Y. & Krashes, M. J. Acts of appetite: neural circuits governing the appetitive, consummatory, and terminating phases of feeding. *Nat. Metab.* **4**, 836–847 (2022).
10. Baver, S. B. et al. Leptin modulates the intrinsic excitability of AgRP/NPY neurons in the arcuate nucleus of the hypothalamus. *J. Neurosci.* **34**, 5486–5496 (2014).
11. Cheng, J. et al. Diet-induced inflammation in the anterior paraventricular thalamus induces compulsive sucrose-seeking. *Nat. Neurosci.* **25**, 1009–1013 (2022).
12. Rossi, M. A. et al. Obesity remodels activity and transcriptional state of a lateral hypothalamic brake on feeding. *Science* **364**, 1271–1274 (2019).
13. Sweeney, P. & Yang, Y. An excitatory ventral hippocampus to lateral septum circuit that suppresses feeding. *Nat. Commun.* **6**, 10188 (2015).
14. Sweeney, P. & Yang, Y. L. An inhibitory septum to lateral hypothalamus circuit that suppresses feeding. *J. Neurosci.* **36**, 11185–11195 (2016).
15. Terrill, S. J. et al. Role of lateral septum glucagon-like peptide 1 receptors in food intake. *Am. J. Physiol. Regul. Integr. Comp. Physiol.* **311**, R124–R132 (2016).
16. Azevedo, E. P. et al. A limbic circuit selectively links active escape to food suppression. *Elife* https://doi.org/10.7554/eLife.58894 (2020).
17. Chen, Z. et al. A circuit from lateral septum neurotensin neurons to tuberal nucleus controls hedonic feeding. *Mol. Psychiatry* **27**, 4843–4860 (2022).
18. Chen, Z. et al. GLP-1R-positive neurons in the lateral septum mediate the anorectic and weight-lowering effects of liraglutide in mice. *J. Clin. Invest.* https://doi.org/10.1172/JCI178239 (2024).
19. Ferrario, C. R. et al. Homeostasis meets motivation in the battle to control food intake. *J. Neurosci.* **36**, 11469–11481 (2016).
20. Vong, L. et al. Leptin action on GABAergic neurons prevents obesity and reduces inhibitory tone to POMC neurons. *Neuron* **71**, 142–154 (2011).
21. Kim, E. R. et al. Hypothalamic non-AgRP, non-POMC GABAergic neurons are required for postweaning feeding and NPY hyperphagia. *J. Neurosci.* **35**, 10440–10450 (2015).
22. Rizzi-Wise, C. A. & Wang, D. V. Putting together pieces of the lateral septum: multifaceted functions and its neural pathways. *eNeuro* https://doi.org/10.1523/ENEURO.0315-21.2021 (2021).
23. Xu, Y. Z. et al. Lateral septum as a melanocortin downstream site in obesity development. *Cell Rep.* https://doi.org/10.1016/j.celrep.2023.112502 (2023).
24. Sheehan, T. P., Chambers, R. A. & Russell, D. S. Regulation of affect by the lateral septum: implications for neuropsychiatry. *Brain Res Brain Res Rev.* **46**, 71–117 (2004).
25. Luo, S. X. et al. Regulation of feeding by somatostatin neurons in the tuberal nucleus. *Science* **361**, 76 (2018).
26. Mohammad, H. et al. A neural circuit for excessive feeding driven by environmental context in mice. *Nat. Neurosci.* **24**, 1132–1141 (2021).
27. Saeed, S., Bonnefond, A. & Froguel, P. Obesity: exploring its connection to brain function through genetic and genomic perspectives. *Mol. Psychiatry* **30**, 651–658 (2025).
28. Bell, C. G., Walley, A. J. & Froguel, P. The genetics of human obesity. *Nat. Rev. Genet* **6**, 221–234 (2005).
29. Locke, A. E. et al. Genetic studies of body mass index yield new insights for obesity biology. *Nature* **518**, 197–206 (2015).
30. Hu, C. X. et al. CellMarker 2.0: an updated database of manually curated cell markers in human/mouse and web tools based on scRNA-seq data. *Nucleic Acids Res* **51**, D870–D876 (2023).
31. Franzén, O., Gan, L. M. & Björkegren, J. L. M. PanglaoDB: a web server for exploration of mouse and human single-cell RNA sequencing data. *Database-Oxford*, https://doi.org/10.1093/database/baz046 (2019).
32. Piñero, J. et al. The DisGeNET knowledge platform for disease genomics: 2019 update. *Nucleic Acids Res* **48**, D845–D855 (2020).
33. Liberzon, A. et al. The molecular signatures database (MSigDB) hallmark gene set collection. *Cell Syst.* **1**, 417–425 (2015).
34. Heiland, M. et al. MicroRNA-335-5p suppresses voltage-gated sodium channel expression and may be a target for seizure control.

Proc. Natl. Acad. Sci. USA **120**, https://doi.org/10.1073/pnas.2216658120 (2023).
35. Spiegel, I. et al. Npas4 regulates excitatory-inhibitory balance within neural circuits through cell-type-specific gene programs. *Cell* **157**, 1216–1229 (2014).
36. Lanore, F. et al. Deficits in morphofunctional maturation of hippocampal mossy fiber synapses in a mouse model of intellectual disability. *J. Neurosci.* **32**, 17882–17893 (2012).
37. Kapur, M. et al. Expression of the neuronal tRNA regulates synaptic transmission and seizure susceptibility. *Neuron* **108**, 193 (2020).
38. Tsanov, M. Differential and complementary roles of medial and lateral septum in the orchestration of limbic oscillations and signal integration. *Eur. J. Neurosci.* **48**, 2783–2794 (2018).
39. Wirtshafter, H. S. & Wilson, M. A. Lateral septum as a nexus for mood, motivation, and movement. *Neurosci. Biobehav R.* **126**, 544–559 (2021).
40. Risold, P. Y. & Swanson, L. W. Chemoarchitecture of the rat lateral septal nucleus. *Brain Res. Brain Res Rev.* **24**, 91–113 (1997).
41. Bean, B. P. The action potential in mammalian central neurons. *Nat. Rev. Neurosci.* **8**, 451–465 (2007).
42. Zhou, X. et al. Hyperexcited limbic neurons represent sexual satiety and reduce mating motivation. *Science* **379**, 820–825 (2023).
43. Chen, G. et al. Cellular and circuit architecture of the lateral septum for reward processing. *Neuron* **112**, 2783–2798 (2024).
44. Paddison, P. J., Caudy, A. A., Bernstein, E., Hannon, G. J. & Conklin, D. S. Short hairpin RNAs (shRNAs) induce sequence-specific silencing in mammalian cells. *Genes Dev.* **16**, 948–958 (2002).
45. Fenalti, G. et al. GABA production by glutamic acid decarboxylase is regulated by a dynamic catalytic loop. *Nat. Struct. Mol. Biol.* **14**, 280–286 (2007).
46. Xu, W. & Sudhof, T. C. A neural circuit for memory specificity and generalization. *Science* **339**, 1290–1295 (2013).
47. Elmquist, J. K., Elias, C. F. & Saper, C. B. From lesions to leptin: hypothalamic control of food intake and body weight. *Neuron* **22**, 221–232 (1999).
48. Di Cesare, M. et al. Trends in adult body-mass index in 200 countries from 1975 to 2014: a pooled analysis of 1698 population-based measurement studies with 19.2 million participants. *Lancet* **387**, 1377–1396 (2016).
49. Carus-Cadavieco, M. et al. Gamma oscillations organize top-down signalling to hypothalamus and enable food seeking. *Nature* **542**, 232–236 (2017).
50. Meyre, D. et al. Is glutamate decarboxylase 2 (GAD2) a genetic link between low birth weight and subsequent development of obesity in children? *J. Clin. Endocrinol. Metab.* **90**, 2384–2390 (2005).
51. Boutin, P. et al. GAD2 on chromosome 10p12 is a candidate gene for human obesity. *Plos Biol.* **1**, 361–371 (2003).
52. Stuber, G. D. & Wise, R. A. Lateral hypothalamic circuits for feeding and reward. *Nat. Neurosci.* **19**, 198–205 (2016).
53. Sweeney, P. & Yang, Y. Neural circuit mechanisms underlying emotional regulation of homeostatic feeding. *Trends Endocrinol. Metab.* **28**, 437–448 (2017).
54. Benarroch, E. E. HCN channels: function and clinical implications. *Neurology* **80**, 304–310 (2013).
55. Senol, E. et al. Brain-wide input-output analysis of tuberal nucleus somatostatin neurons reveals hierarchical circuits for orchestrating feeding behavior. *Nat. Commun.* **16**, 5627 (2025).
56. Xu, Y. et al. Identification of a neurocircuit underlying regulation of feeding by stress-related emotional responses. *Nat. Commun.* **10**, 3446 (2019).
57. Kanter, R. & Caballero, B. Global gender disparities in obesity: a review. *Adv. Nutr.* **3**, 491–498 (2012).
58. Oraha, J., Enriquez, R. F., Herzog, H. & Lee, N. J. Sex-specific changes in metabolism during the transition from chow to high-fat diet feeding are abolished in response to dieting in C57BL/6J mice. *Int J. Obes. (Lond.)* **46**, 1749–1758 (2022).
59. Simon, R. C. et al. Opioid-driven disruption of the septum reveals a role for neurotensin-expressing neurons in withdrawal. *Neuron* **113**, 2325–2343 e2329 (2025).
60. Slyper, M. et al. A single-cell and single-nucleus RNA-Seq toolbox for fresh and frozen human tumors. *Nat. Med* **26**, 792–802 (2020).
61. Hao, Y. et al. Dictionary learning for integrative, multimodal and scalable single-cell analysis. *Nat. Biotechnol.* **42**, 293–304 (2024).
62. McGinnis, C. S., Murrow, L. M. & Gartner, Z. J. DoubletFinder: doublet detection in single-cell RNA sequencing data using artificial nearest neighbors. *Cell Syst.* **8**, 329–337 e324 (2019).
63. Stuart, T. et al. Comprehensive Integration of single-cell data. *Cell* **177**, 1888–1902 e1821 (2019).
64. clusterProfiler: an R package for comparing biological themes among gene clusters. *OMICS: A J. Integr. Biol.* **16**, 284–287 (2012).
65. Aibar, S. et al. SCENIC: single-cell regulatory network inference and clustering. *Nat. Methods* **14**, 1083 (2017).
66. Zhu, Y., Wienecke, C. F., Nachtrab, G. & Chen, X. A thalamic input to the nucleus accumbens mediates opiate dependence. *Nature* **530**, 219–222 (2016).
67. Cai, D. J. et al. A shared neural ensemble links distinct contextual memories encoded close in time. *Nature* **534**, 115–118 (2016).
68. Zhou, P. et al. Efficient and accurate extraction of in vivo calcium signals from microendoscopic video data. *Elife* https://doi.org/10.7554/eLife.28728 (2018).
69. Pnevmatikakis, E. A. & Giovannucci, A. NoRMCorre: an online algorithm for piecewise rigid motion correction of calcium imaging data. *J. Neurosci. Methods* **291**, 83–94 (2017).
70. Yang, T. et al. Plastic and stimulus-specific coding of salient events in the central amygdala. *Nature* **616**, 510–519 (2023).
71. Taylor, S. C. et al. The ultimate qPCR experiment: producing publication quality, reproducible data the first time. *Trends Biotechnol.* **37**, 761–774 (2019).
72. Chen, Z. Y. et al. Real-time effects of nicotine exposure and withdrawal on neurotransmitter metabolism of hippocampal neuronal cells by microfluidic chip-coupled LC-MS. *Chin. Chem. Lett.* **33**, 3101–3105 (2022).
73. Chen, T. et al. The genome sequence archive family: toward explosive data growth and diverse data types. *Genomics Proteom. Bioinforma.* **19**, 578–583 (2021).
74. Members, C.-N. & Partners. database resources of the national genomics data center, China National Center For Bioinformation in 2022. *Nucleic Acids Res* **50**, D27–D38 (2022).

Acknowledgements

The authors thank E.N., G.B., and X.C. for insightful suggestions and discussions. This work was supported by the Strategic Priority Research Program of the Chinese Academy of Sciences (XDB0930000), the Major Project of the Science and Technology Innovation 2030 of China (2021ZD0202103), the National Natural Science Foundation of China (82425023, 82171492, 32400840), the Yunnan Technological Innovation Centre of Drug Addiction Medicine (202305AK340001), the Department of Science and Technology of Guangdong Province (2023B1515040009, 2023A1515110576), the Technology and Innovation Commission of Shenzhen (RCJC20200714114556103), the Innovative Research Team of High-Level Local Universities in Shanghai, and the Analytical and Testing Center of Shenzhen Institute of Advanced Technology (SIAT).

Author contributions

Y.Z. and G.C. conceptualized and designed the study. S.J., S.L. and G.C. conducted the majority of the experiments and the data analysis. S.J. and S.L. were responsible for the bioinformatics analysis and calcium imaging. S.J. and H.J. conducted the electrophysiological experiments and data analysis. X.W. contributed to the generation of experimental

mice. J.B., L.W., F.L., and B.C. participated in data interpretation and discussion. Y.Z., G.C. and S.J. wrote the manuscript with input from all authors. All authors reviewed and approved the final version of the manuscript.

Competing interests
The authors declare no competing interests.

Additional information
Supplementary information The online version contains supplementary material available at https://doi.org/10.1038/s41467-025-68010-x.

Correspondence and requests for materials should be addressed to Gaowei Chen or Yingjie Zhu.

Peer review information *Nature Communications* thanks Ivett Gabriella and the other, anonymous, reviewer(s) for their contribution to the peer review of this work. A peer review file is available.